Department of Physical Geography and Ecosystems Analysis, Lund University

Seminar Report Series No. 97

Wind Throw Damages on Forests – Frequency and Associated Pressure Patterns 1961-1990 and in a Future Climate Scenario

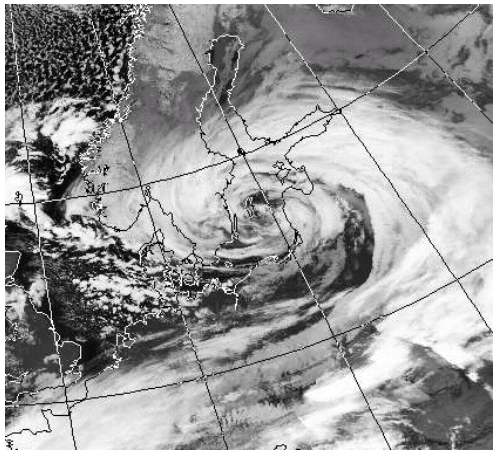

Jacob Svensson

Diploma work in Physics, 20 credits
Tutor: Lars Bärring

2003
Department of Physical Geography and Ecosystems Analysis,
Lund University
Sölvegatan 12, S-221 00 Lund,
Sweden

Abstract

Many different simulations of the future climate have shown a probable change of the climate of the earth, mainly caused by anthropogenic emissions. A change in the climate influences many parameters. In this report the frequency of extreme wind situations in Southern Sweden and associated pressure patterns during the period 1961 to 1990 are compared to the conditions for the years 2070-2099.

Different methods are tested. The first attempt is based on analog situations. Selected situations associated with observed strong winds during the period 1961-1990 are identified. Reanalyzed mean sea level pressure data from the National Centers for Environmental Predictions (NCEP) is used to find the pressure field associated to each storm situation. Analog situations to these days are then searched in the Hadley Center's circulation model HadAM3, present day (COM) and future conditions (A2) simulations. The second attempt is based on calculated geostrophic wind. Days with a geostrophic wind exceeding 25 m/s in the NCEP dataset are divided into groups by cluster analysis. Days in the HadAM3COM and A2 simulations that are associated with geostrophic wind speeds over 25 m/s are then divided into these classes. The frequency of each group in HadAM3COM and HadAM3A2 is then compared. Principal component analysis is applied to the days in each run associated to strong geostrophic winds, and the main principal components of the present day and future simulations are compared.

The first method is not able to detect any significant differences between the two different simulated periods. The second revealed a slight decrease in total storm frequency, most notable at occasions with a widespread low over Northern Scandinavia and for easterly storms with a high over northern Finland and Russia. No significant changes between HadAM3COM and HadAM3A2 can be seen in their main principal components.

Keywords: analog, climate change, climate model, extratropical cyclone, extreme wind, forest damage, geostrophic wind, pressure pattern, southern Sweden, storm damage, windstorm

Sammanfattning

Flera olika klimatsimuleringar har visat på en sannolik förändring av jordens klimat, till största delen beroende på utsläpp orsakade av mänsklig aktivitet. Eftersom klimatet påverkar såväl ekosystem som livsmiljö är det av största intresse att kartlägga vilka konsekvenser en eventuell klimatförändring kan få. Även om människans vardag för det mesta påverkas av det normala klimatet är det förändringen av extrema situationer som ofta hamnar i blickfånget. Detta arbete är ett bidrag till studierna av en eventuell förändring av extrema vädersituationer. Fokus i arbetet är riktat mot extrema vindar som kan orsaka betydande skador på till exempel skogsbestånd och som i högsta grad kan påverka samhället i stort.

För att simulera eventuella klimatförändringar har flera globala cirkulationsmodeller (GCM) utvecklats. I detta arbete har data använts från modellkörningar vid den brittiska vädertjänstens klimatcenter, Hadley Centre. En global cirkulationsmodell för atmosfären som använder randvärden från en kopplad havs- och atmofärsmodell har körts för två perioder. Den första perioden, åren 1961-1990, används här för att jämföra modellen med observationer och benämns 'common period' (COM). Den andra perioden, 2070-2099, är ett simulerat framtida klimat med ett scenario för utsläpp av växthusgaser som kallas A2.

Syftet med arbetet är att jämföra frekvensen av extrema vindsituationer i södra Sverige och den därtill associerade tryckbilden under perioden 1961-01-01 till 1990-12-31 med frekvens och därtill associerad tryckbild för extrema vindsituationer i ett framtida klimatscenario för perioden 2070-2099. Olika metoder har testats. Den första bygger på analoga situationer. Först identifierades datum för ett antal observerade kraftiga stormar under perioden 1961-01-01 till 1990-12-31. Återanalyserade data för trycket vid havsnivå från den amerikanska vädercentralen NCEP användes för att hitta en till stormtillfällena associerad trycksituation och geostrofisk vind. Därefter gjordes en sökning av liknande situationer till dessa både i perioden 1961-1990 och 2070-2099 i data från klimatmodellen HadAM3. Det andra försöket baserades på beräknad geostrofisk vind. Den geostrofiska vinden är den vind som krävs för att Corioliskraften skall balansera tryckgradientkraften, dvs ett luftpaket följer en bana parallell med isobarerna. Dagar med en beräknad geostrofisk vind på mer än 25 m/s i NCEP-data grupperades med hjälp av klusteranalys, där dagar som liknar varndra tillräckligt mycket hamnar i samma grupp. Dagar i HadAM3COM resp HadAM3A2 som är associerade med lika höga vindhastigheter klassificeras sedan in i dessa grupper. Genom att jämföra frekvensen av respektive grupp i respektive simulering kan eventuella förändringar avslöjas i tryck-bilden vid blåsiga tillfällen. Vidare jämfördes de viktigaste principalkomponenterna från blåsiga situationer i HadAM3COM och HadAM3A2 för att hitta eventuella skillnader.

Den först applicerade metoden kunde inte uppvisa några signifikanta skillnader i stormtillfällen mellan de båda modellkörningarna. Den andra visade en viss minskning totalt i stormtillfällen. Detta var mest markant för stormtillfällen associerade med ett utbrett lågtryck över norra Skandinavien samt för ostliga stormar associerade med ett högtryck över N Finland och Ryssland. Denna skillnad återpeglades inte i analysen av principalkomponenter.

Table of contents

1. Introduction

1.1. Background

During the last decade the question of an anthropogenic induced climate change has been one of the most discussed questions in environmental science and politics. Local climate has great impact on both the ecological and the anthropogenic environment. Changes in climate may cause droughts or floods, biotopes and species may change or disappear, human health and well-being is affected. Many reports have been written about impact on temperature, precipitation etc. A brief review of the impact of climate changes is found in the annual report for 2002 from SWECLIM (Persson, 2002).

The wind climate in Sweden is influenced by mid-latitude synoptic scale weather phenomena, as moving frontal cyclones and polar lows. West winds are dominating in the south of Sweden. The summertime heating moves the polar front northward, which gives a seasonal mean north-south oscillation of the front. Most of the extreme wind situations are associated to a deep moving low. Different types of cyclones are observed, including ordinary frontal disturbances, polar lows and lows caused by upper level jet streaks. Normally highest wind speed is measured at coastal stations since the friction over sea is less than over land, but most severe forest damages are often found in more continental regions. Observations and many reports show an increase in storm frequency of the North Atlantic and NW Europe during the last decades of the 20:th century. Studies of the long-term variation of wind climate is done by e.g. Alexandersson et al. (1998), over NW Europe and by Franzén (1991) for the Swedish west coast. Both show big differences over decades, with a frequency increase in the late 20:th century but no long-term trend. Neither did Heino et al. (1999) find any long-term trend in the wind climate over central and northern Europe. The WASA group (1998) did neither find any trend during this century nor for a future climate scenario, although a frequency difference of storms where higher at the start and end than in the middle of the 20:th century.

In Ch. 2.9 the influence of a climate change on cyclones and cyclogenesis is described. It is found that the temperature gradients between high and low latitudes seems to weaken at low level and to increase at upper levels. The net effect in a climate scenario with increased green house gases (GHG) varies in different models. A couple of studies of the frequency and strength of mid-latitude depressions in models of a future climate change have been employed. Ulbrich and Christoph (1999) found an increase in storm track activity over Western Europe due to increased upper level baroclinity. Knippertz et al. (2000) did not find any total frequency change for the North Atlantic and European area, but a decrease of weak cyclones and an increase of deep cyclones with core pressures below 970 hPa. Beersma et al. (1997) on the other hand found a slight decrease in the frequency of total depressions, but an increase over the North Sea and Gulf of Biscay. In fact, although the change of global frequency of extratropical cyclones differs between the models, many models seem to agree of an increase of deep cyclones over the Northwest parts of Europe.

1.2. Objectives and structure of work

The Department of Physical Geography and Ecosystems Analysis at Lund University is involved in the MICE (Modelling the Impact of Climate Extremes) research project founded by the European Union with the purpose to identify likely changes in the occurrences in extremes of rainfall, temperature and windstorm over Europe due to global warming with information from climate models. The contribution from Lund University to this project is to evaluate the impact of extreme weather on North European forests, involving e.g. the occurrence of heavy snowfall and windstorms. The aim of this report is to determine whether the likeliness of extreme winds causing forest damages are likely to change in a future climate scenario and if the pressure pattern at stormy occasions is different from present day.

To determine whether the probability of forest damages will increase or not in a future climate scenario, many parameters have to be taken into account. The wind climate is only one of many parameters influencing the mechanical parameters of trees. Studies of the mechanics of forest damages have been employed by e.g. Talkkari et al. (2000). Anyway, storm winds are the only factor forcing forest wind-throw, other factors only determines the vulnerability to wind damages (Nilsson, 2003). A more extensive report of wind throw damages is found in Nilsson (2003).

Mean sea level pressure data from United Kingdom's meteorological office's, UKMO:s, third atmospheric climate model HadAM3H driven with the preferences from IPCC:s emission scenario A2 for the period 2070-99 was used to compare the future extreme wind climate over southern Sweden with the extreme wind climate from 1961-01-01 to 1990-12-31. IPCC:s A2 scenario is a kind of worst case situation, with a very heterogeneous world and rather a slow and regionally differentiated economic growth, and increased emissions of green house gases (Watson et al, 2002). Data from the control run HadAM3COM, which was run from 1860 to present day using real atmospheric parameters as well as reanalyzed data from NCEP covering most of Europe were used for the period 1961-01-01 to 1990-12-31. Model data from the Hadley Center and NCEP-data were provided by the MICE project.

Two different methods to investigate storm frequencies and their corresponding pressure patterns were tested. The first is based on analog situations, the principle in detailed described by Lorenz (1969). Different interpretations are used in climatologic research, e.g. estimation of precipitation (Zorita et al, 1995) and estimation of transport of macroturbulent heat (Luksch and von Storch, 1999). The NCEP pressure field of days with documented forest or environmental wind caused damages was combined into clusters, and analog situations based in the model HadAM3COM and HadAM3A2 are searched. The frequency of analogs and the distribution into clusters were then analyzed for the different climate situations.

The second method used, described in more detail in Ch. 3, is a different interpretation of the analog method based on principal component analysis (PCA) and cluster analysis. First, geostrophic wind was introduced and is validated against measurements to

determine if it is a useful tool to describe strong real and measured ground (10 m) wind. Thereafter PCA was done on days with strong geostrophic winds, and these situations were divided into different clusters. Stormy days in HadAM3COM and HadAM3A2 were then searched and their most important PC:s are identified. Storm situations were then associated to different clusters to find a frequency distribution.

In both methods the geostrophic wind approximation was used to calculate wind speeds from pressure data. Geostrophic wind is the wind speed required for the Coriolis force to balance the pressure gradient. By applying this relation, the wind can be calculated with only information about the current pressure field. The geostrophic wind approximation disregards boundary layer effects as friction and turbulence, centrifugal force, isallobaric winds, mesoscale phenomena as convection and downdrafts etc. In a stationary situation the calculations of geostrophic wind tend to overestimate the average ground wind speeds due to friction and turbulence, although wind gusts may reach higher values. Channeling may cause locally higher winds than the geostrophic wind. Rapidly developing small-scale phenomena such as thunderstorms is not resolved by the geostrophic approximation and may therefore be underestimated. High-resolution models can give a quite accurate estimation of the wind at a certain height using the theories for the surface and boundary layers, but they are computationally demanding. Anyway, here the geostrophic approximation was shown to be a useful tool to describe the occurrence of strong surface winds. Geostrophic wind can also be used to replace inconsistent or inhomogeneous time-series of wind observations (Alexandersson et al., 1998).

An attempt to investigate changes in strong cyclonic development was done, but did unfortunately not succeed. The method required a temporal resolution higher than the 24 h time step in the available dataset.

1.3 Structure of the report

In Ch. 2 a presentation of relevant meteorological concepts is found, including geostrophic wind, quasi-geostrophic theory, baroclinic development and cyclogenesis. In Ch. 3 the data and in Ch. 4 the method used is described in more detail. Ch. 5 contains the results and Ch. 6 is a discussion of achieved results. The appendix consists of a deeper explanation of principal component analysis together with plots for validation of geostrophic winds, tables and pressure maps.

2. Geostrophic wind and cyclones

This chapter is a basic review of important meteorological concepts for winds and cyclones. First the governing equations for atmospheric motion are introduced. The simpler geostrophic wind approximation is then introduced and explained. Geostrophic wind is used in this report to calculate winds from a pressure field. Thereafter the geopotential height is introduced, which is an important parameter to understand the influence of temperature on the stream pattern. As most severe storm days are associated to cyclones, the understanding of the dynamics of cyclones is important to understand the impact of a climate change on strong winds. Here the theories for cyclonic development is described with the use of quasi-geostrophic and baroclinic theory. At the end of the chapter severe forms of cyclogenesis such as bombs and polar lows are described.

2.1 Equations of motion

A wind is a result from cooperating forces on an air parcel. The forces working on an air particle in the atmosphere is pressure, friction and the Coriolis force, a virtual force caused by a rotating coordinate system. The equations of motion for a particle in a rotating system can be written (Holton 1992, p 37):

$$\frac{Du}{Dt} - \frac{uv\tan\phi}{a} + \frac{uw}{a} = -\frac{1}{\rho}\frac{\partial p}{\partial x} + 2\Omega v\sin\phi - 2\Omega w\cos\phi + F_{rx} \tag{2.1}$$

$$\frac{Dv}{Dt} + \frac{u^2\tan\phi}{a} + \frac{vw}{a} = -\frac{1}{\rho}\frac{\partial p}{\partial y} + 2\Omega u\sin\phi + F_{ry} \tag{2.2}$$

$$\frac{Dw}{Dt} - \frac{u^2+v^2}{a} = -\frac{1}{\rho}\frac{\partial p}{\partial z} - g + 2\Omega u\cos\phi + F_{rz} \tag{2.3}$$

where

- u is the speed in x-direction (West - East)
- v *is* the speed in y-direction (South - North)
- w is the vertical speed
- a is the distance to the center of the earth
- F_r is frictional force
- ϕ is the latitude
- p is the pressure

and

$$\frac{D}{Dt} = \frac{\partial}{\partial t} + u\frac{\partial}{\partial x} + v\frac{\partial}{\partial y} + w\frac{\partial}{\partial z}$$

These equations together with the continuity equation and the thermodynamic equation are the governing equations, which give an analytically unsolvable set of equations that determines the winds, the development and character of weather systems etc.

2.2 Geostrophic wind approximation

Although the basic equations of motion look quite simple, there are too many degrees of freedom for an exact solution. One attempt to reduce the degrees of freedom is to apply a scale analysis, where characteristic scales for each variable in Eq. 2.1-2 are defined and the magnitude of the factors in those equation are determined. Typical scales for a synoptic system is (Holton, 1992, p 39):

- $V \sim U \sim 10$ m s^{-1} horizontal velocity (i.e. wind) scale
- $W \sim 1$ cm s^{-1} vertical velocity scale
- $L \sim 10^6$ m length scale [*~1/(2π)* wavelength]
- $H \sim 10^4$ m depth scale
- $\delta P/\rho \sim 10^3$ m^2 s^{-2} horizontal pressure fluctuation scale
- $L / U \sim 10^5$ s time scale
- $\nu \sim 10^{-5}$ m^2 s^{-1} viscosity
- $f_0 \sim 10^{-4}$ s^{-1} Coriolis parameter

The magnitude of each term is then found in Tab. 2.1.

Tab. 2.1: Scale analysis applied to Eq. 2.1 and 2.2. The typical magnitude of each term is found in the last line. (From Holton 1992, p 39).

	A	B	C	D	E	F	G
x - Eq.	$\frac{Du}{Dt}$	$-2\Omega v\sin\phi$	$+2\Omega w\cos\phi$	$+\frac{uw}{a}$	$-\frac{uv\tan\phi}{a}$	$=-\frac{1}{\rho}\frac{\partial p}{\partial x}$	$+F_{rx}$
y - Eq.	$\frac{Dv}{Dt}$	$+2\Omega v\sin\phi$		$+\frac{vw}{a}$	$-\frac{u^2\tan\phi}{a}$	$=-\frac{1}{\rho}\frac{\partial p}{\partial y}$	$+F_{ry}$
Scales	$\frac{U^2}{L}$	$f_0\ U$	$f_0\ W$	$\frac{UW}{a}$	$\frac{U^2}{a}$	$\frac{\partial p}{\rho L}$	$\frac{\nu U}{H^2}$
(m s^{-2})	10^{-4}	10^{-3}	10^{-6}	10^{-8}	10^{-5}	10^{-3}	10^{-12}

With the scales used the main terms of Eq. 2.1 and 2.2 then reduce to (Holton, 1992, p 40):

$$fu \approx -\frac{1}{\rho}\frac{\partial p}{\partial y} \tag{2.4}$$

$$-fv \approx -\frac{1}{\rho}\frac{\partial p}{\partial x} \tag{2.5}$$

which defines the geostrophic approximation, where f is the Coriolis parameter

$$f = 2 \cdot \Omega \cdot \sin(\phi)$$

where Ω is the angular velocity of the earth and ϕ the latitude. The geostrophic wind is the wind determined by Eq. 2.4-5. This means that the geostrophic wind is determined only by the horizontal pressure gradient, the Coriolis parameter and the density. From these equations it is seen that the geostrophic wind is counterclockwise, or cyclonic around a low-pressure area and clockwise, or anticyclonic, around a high-pressure area.

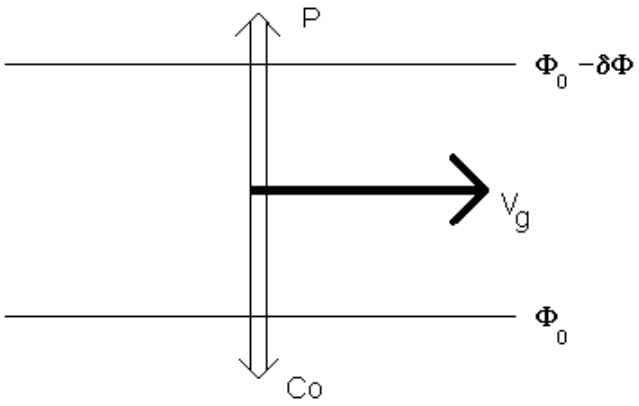

Fig. 2.1: Balance of forces for geostrophic equilibrium. The pressure force is designated P and the Coriolis force Co. The geostrophic balance is shown using geopotential height instead of pressure. (Holton, 1992, p 64).

If the magnitudes of the terms removed in the scale analysis above are larger than assumed here, the geostrophic approximation is not valid. This is the case in e.g. short time and small scale weather disturbances as turbulence and topographically induced waves. The geostrophic approximation is neither valid in convective systems such as thunderstorms as the time scale there is significantly shorter (a couple of hours) and the vertical speed much larger (up to 10 m/s) than what is assumed in the scale analysis. Anyway, for a regular cyclone, where the time and length scale are in the same order as in the scale analyses mentioned above, the geostrophic wind is not too bad, but mostly too high, approximation for the real wind, at least above the boundary layer. The geostrophic approximation does not include friction that usually decreases the wind speed close to the ground and causes the air in the boundary layer to converge into the low-pressure area and to diverge from the high-pressure area. As seen later in this report, the geostrophic wind based on mean sea level pressure data shows a satisfying correlation with measurements on ground stations.

2.3 Geopotential height and thermal wind

Different ways to describe the coordinate in height are used in meteorology. In many meteorological interpretations isobaric coordinates, where the pressure *p* is used as vertical coordinate instead of the height, *z*, is used to simplify the equations. When isobaric coordinates are used, the height of a certain pressure is described as geopotential height.

For an atmosphere without any vertical motions the pressure difference on an infinitesimal height difference can be written as the mass change over that height difference:

$$\frac{\partial p}{\partial z} = -\rho g \tag{2.6}$$

This is the hydrostatic equation. If integrated from a certain level to the top of the atmosphere we get:

$$p(z) = \int_z^\infty \rho g \, dz$$

The geopotential at height z is given by:

$$\Phi = \int_0^z g \, dz \tag{2.7}$$

From the equation of state for an ideal gas we get:

$$p = \rho R T \tag{2.8}$$

If this relation is inserted in the hydrostatic equation we get:

$$\frac{\partial p}{\partial z} = -\frac{pg}{RT} \quad \Leftrightarrow \quad \frac{RT}{p}\frac{\partial p}{\partial z} = -g \tag{2.9}$$

The difference in geopotential between two pressure levels can then be written:

$$\Phi(z_2) - \Phi(z_1) = R\int_{p_2}^{p_1} T \, d \, \ln \, p \tag{2.10}$$

That means that the thickness between two pressure levels is a function of the temperature in that layer. A warm column of air gives greater distance between pressure levels than a cold column. The geopotential height is defined as $Z \equiv \Phi(z) / g_0$, where g_0 is the global average of the gravity at mean sea level. In isobaric coordinates the geostrophic wind can be written:

$$u_g = -\frac{1}{f}\frac{\partial \Phi}{\partial y} \tag{2.11}$$

$$v_g = \frac{1}{f}\frac{\partial \Phi}{\partial x} \tag{2.12}$$

Combined with Eq. 2.10 these equations states that the geostrophic wind changes with height if a horizontal temperature gradient is present. The vertical wind shear caused by

temperature differences is important to explain large-scale circulations and the theories behind cyclonic development.

2.4 Quasi-geostrophic approximation

The governing equations have too many degrees of freedom to admit a reasonably simple solution to describe a evolving cyclone. Therefore, a simpler model has been devised to provide less computational demanding calculations and simpler qualitative understanding, the quasi-geostrophic theory. A deeper explanation and derivation of this theory is found e.g. Holton (1992) or Carlson (1998). The result of this approximation is summarized in the "geopotential tendency equation" or "χ-equation", and the "ω-equation", where

$$\chi \equiv \frac{\partial \Phi}{\partial t}$$

and ω is the vertical velocity in pressure coordinates (notice that positive ω means negative vertical velocity), and can be written (Holton 1992, p 159 and p167)

$$\underbrace{\left[\nabla^2 + \frac{\partial}{\partial p}\left(\frac{f_0^2}{\sigma}\frac{\partial}{\partial p}\right)\right]}_{\text{A}}\chi = \underbrace{-f_0 \mathbf{V}_g \cdot \nabla\left(\frac{1}{f_0}\nabla^2\Phi + f\right)}_{\text{B}} - \underbrace{\frac{\partial}{\partial p}\left[-\frac{f_0^2}{\sigma}\mathbf{V}_g \cdot \nabla\left(-\frac{\partial \Phi}{\partial p}\right)\right]}_{C} \qquad (2.13)$$

$$\underbrace{\left(\nabla^2 + \frac{f_0^2}{\sigma}\frac{\partial^2}{\partial p^2}\right)}_{\text{D}}\omega = \frac{f_0}{\sigma}\frac{\partial}{\partial p}\underbrace{\left[\mathbf{V}_g \cdot \nabla\left(\frac{1}{f_0}\nabla^2\Phi + f\right)\right]}_{\text{E}} + \underbrace{\frac{1}{\sigma}\nabla^2\left[\mathbf{V}_g \cdot \nabla\left(-\frac{\partial \Phi}{\partial p}\right)\right]}_{\text{F}} \qquad (2.14)$$

The parameter σ is called static stability and is a measurement of the ability of an air parcel to undergo vertical motions under actual atmospheric conditions. A low value of static stability means unstable atmospheric conditions and enhanced vertical motion. Eq. 2.13 is a diagnostic equation that for a given geopotential field Φ and geostrophic wind pattern $\mathbf{V}_g$ determines how much the geopotential at a certain level changes with time. Disturbances in the atmosphere can be regarded as Fourier components, a summation of sinus or cosinus waves with different wave numbers. For a sinusoidal or cosinusoidal wave pattern Eq. 2.13 and 2.14 can be written in a more qualitative form (Holton, 1992, p 177):

Geopotential tendency equation (*Eq 2.13*):

$$\text{Geopotential}\begin{pmatrix}\text{fall}\\ \text{rise}\end{pmatrix} \propto \begin{pmatrix}+\\ -\end{pmatrix}\text{vorticity advection} + \begin{pmatrix}\text{cold}\\ \text{warm}\end{pmatrix}\text{advection decreasing with height}$$

Omega equation (*Eq 2.14*):

$$\begin{pmatrix}\text{Rising}\\ \text{Sinking}\end{pmatrix}\text{motion} \propto \text{rate of increase with height of} \begin{pmatrix}+\\ -\end{pmatrix}\text{vorticity advection}$$
$$+\begin{pmatrix}\text{warm}\\ \text{cold}\end{pmatrix}\text{advection}$$

To maintain the angular momentum in areas of positive vorticity advection air has to be lifted. If air is lifted from the ground and advected away at higher altitudes, the geopotential falls and the pressure at ground level decreases, as the transport through the ground is zero and not enough air can be transported from the surroundings into the low-pressure center due to geostrophy. The development and movement of lows and highs are closely connected to the quasi-geostrophic equations. A qualitative interpretation of these equations is done in the next chapters to explain the driving forces of cyclogenesis.

2.5 The concept of Baroclinic instability

There is a well-known phrase highlighting the instability of the atmospheric circulation saying something like 'the wing beats of a butterfly in South America may cause a storm in Scandinavia'. Under certain atmospheric conditions small disturbances becomes unstable and amplify. For a cyclone that means a pressure fall and an increase of pressure gradient. The cause of amplifying disturbances in the mid-latitudes is called baroclinic instability. Here, just a short review of necessary conditions for baroclinic instability is presented. For a deeper explanation see Holton (1991) Ch. 8.

In the ideal baroclinic case the terms in the geopotential tendency equation and the omega-equation interact. That is, the structure of an amplifying wave shows the same pattern as shown in Fig. 2.2 and described in Tab. 2.1. Positive vorticity advection that increases with height in B causes air to rise to conserve angular momentum at upper levels. Cold and warm advection in A respective C amplifies the upper level trough and ridge, which amplifies the vorticity advection and increases the vertical velocity in B. This causes a pressure fall at ground level in B, and the temperature advection at A and C enhances etc. It can be shown that for a model consisting of two different atmospheric layers the 1000 – 500 hPa temperature lags the 500 hPa wind field with ¼ wavelength model when ideal conditions for baroclinic development is present. Then both the northward transport of warm air east of the middle layer trough and the southward advection of cold air west of the middle layer trough are maximized (Holton 1992, p 249). The result is cold advection below the upper level trough that amplifies. As observed in e.g. polar lows waves can amplify with only one term active in Eq. 2.13 and 2.14, as long as the forcing is strong enough. In Karlsson (1988) two different ways of cyclogenesis are described; type A, that is the classical small baroclinic wave disturbance that evolves to a deep cyclone, and type B, where a upper level trough with strong vorticity advection creates a surface low. Although the surrounding might be baroclinic (with a horizontal temperature gradient) in type B cyclones, the development is

barotropic (without the influence of a horizontal temperature), and is caused by barotropic instability (Bluestein 1993, p 112) The model of cyclonic evolution described in the next section, is somewhat of a combination of these.

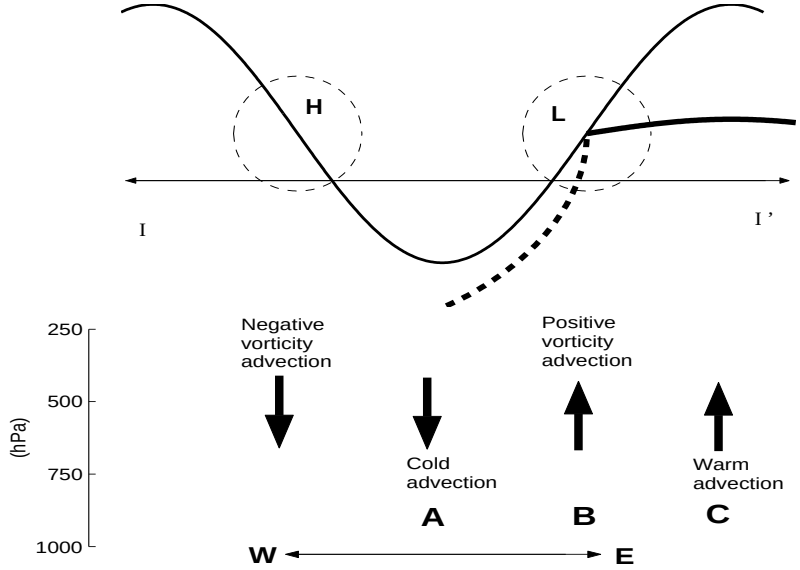

Fig. 2.2: Secondary circulation associated with a developing baroclinic wave. Top: Horizontal view. Schematic 500-mb contour (solid line), 1000-mb contours (dashed lines), and surface fronts (thick solid line – warm front, thick dashed line – cold front). Bottom: Vertical profile through the line II' indicating the vertical motion field (Redrawn after Holton, 1992, p 178).

Tab. 2.1: Characteristics of a developing baroclinic disturbance. The letters A, B and C refers to Fig. 2.3. ξ is the relative vorticity. (After Holton, 1992, p 179).

Physical parameter	**A 500-hPa trough**	**B Surface low**	**C 500-hPa ridge**
$\partial(\delta\Phi)/\partial t$ (500-100 hPa)	Negative (thickness advection partly adiabatic cancelled by warming)	Negative (adiabatic cooloing)	Positive (thickness advection partly canceled by adiabatic cooling)
w (500 hPa)	Negative	Positive	Positive
$\partial\Phi/\partial t$ (500 hPa)	Negative (differential thickness advection)	Negative (vorticity advection)	Positive (differential thickness advection)
$\partial\zeta/\partial t$ (1000 hPa)	Negative (divergence)	Positive (convergence)	Positive (convergence)
$\partial\zeta/\partial t$ (500 hPa)	Positive (convergence)	Positive (advection partly canceled by divergence)	Negative (divergence)

2.6 Available potential Energy (APE)

Due to the difference in incoming solar radiation on the equator and at higher latitudes, the temperature near the ground is much lower in the polar areas than closer to the equator. Hence the distance between two pressure levels is lower at higher latitudes, and at sufficiently high altitudes a permanently lower value of geopotential height are found than to the south. The result is a zonally averaged geostrophic wind, blowing from east to west at higher altitudes in the midlatitudes. The kinetic energy in this average wind field is a conversion of the zonally averaged available potential energy (APE) (Holton 1992, p 245). As the driving force for the atmospheric circulation is the temperature difference between north and south, the absolute temperature (or total energy in the air) is of subordinate importance. APE is a measurement of how far from a homogeneous temperature field the current state is, i.e. the maximum energy that can be converted into kinetic energy. Near a frontal zone, the temperature gradient is strong and the APE is high. APE can also be produced by adiabatic heating of descending air and cooling of ascending air. For a wave to amplify, the kinetic energy in the disturbance must increase, either from drawing kinetic energy from the zonally averaged wind field, as in the case of barotropic instability, or, as in the case of baroclinic instability, by conversion from APE to kinetic energy (illustrated in Grotjahn (1993), Fig. 4.26 p 149). Available potential energy is converted into kinetic energy if heavy (cold) air sinks and light (warm) air rises, the center of mass is lowered and kinetic energy is released (Holton 1992, p 248). In the classical Norwegian front-cyclone model warm air is rising at the warm front and cold air sinking behind the cold front (Carlson 1998, Fig. 10.1), and APE is converted to kinetic energy. As long as the conversion to kinetic energy is greater than the frictional loss, the wind associated with the disturbance increases. When the energy conversion weakens or disappears, friction will decrease winds and causes pressure differences to be filled, and the cyclone or anticyclone disappears.

2.7 Cyclogenesis

In midlatitudes the most severe weather phenomena on synoptic scale is caused by moving cyclones. Deep cyclones and their associated fronts often bring precipitation and strong winds. One of the first models of evolution of cyclones was developed by J. Bjerknes and H. Solberg in the 1920's, and is still used in order to get a qualitative picture of the development of cyclones. The structure of a developing cyclone according to this model is shown in Fig. 2.3 and the vertical view of the development is shown in Fig. 2.4.

The qualitative description of the omega equation combined with the theory for baroclinic development provides a powerful tool to explain cyclonic development. Recall Fig. 2.2 and Tab. 2.1. If an area with high vorticity advection, e.g. downstream a height trough, is located above a ground frontal wave, the omega-equation shows that air will rise, with following pressure decrease at the surface. This pressure decrease causes a cyclonic movement near the ground, and strong temperature advection where warm air descends over the warm front, east of the low center, and therefore rising motion. In similar way, cold advection appears at the cold front with sinking motion as consequence.

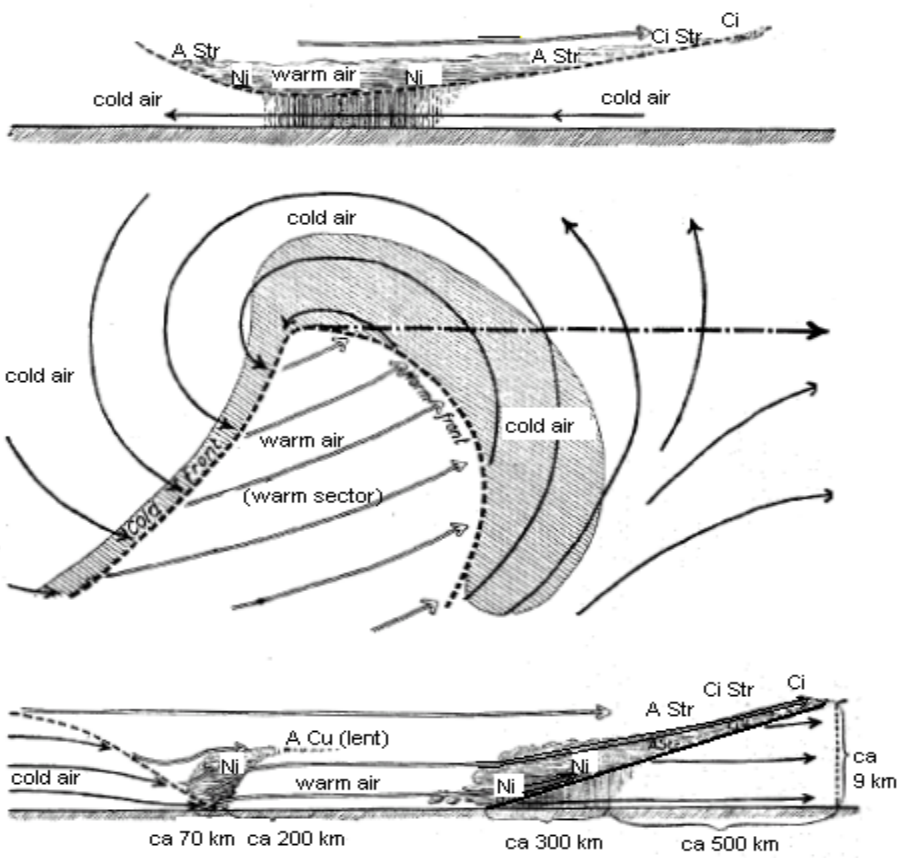

Fig. 2.3: Idealized cyclone according to the Norwegian model. a): Cut along the dash dotted line through the cold sector in b). Cloud formation from right, first appears high cirrus clouds, followed by a thin cirrostratus, that thickens and pass into altostratus. Precipitation close to the cyclone center or at the warm front originates from Nimbostratus-clouds. Warm air rising over the cold air causes precipitation and clouds. b). Vertical view showing airflow, precipitation, fronts and air masses. c). Horizontal cut showing the cold front, warm sector, warm front and cold sector. (After Bjerknes and Solberg (1926))

Thus, surface pressure decreases east-northeast of the low, and increases south-southeast of the low. The low pressure center moves towards the area of greatest pressure fall. The cyclone tends to move in north-east direction. The vertical motion also affects the height geopotential pattern; the sinking motion west of the surface low deepens the height trough and rising close to the warm front causes an increase in geopotential height east or northeast of the surface pressure center. The result is enhanced vorticity advection in the area above the surface low center. This is the baroclinic development. The change in upper level flow creates even more absolute vorticity advection over the surface low-pressure area, and enhanced cyclonic development (Carlson 1998, 232). The decaying of the cyclone is not caused by the occlusion, as imposed in the Norwegian model, but rather a consequence of thickness minimum north-west of the frontal cyclone caused by ascending air in association with pole- and westward expansions of cloud mass and temperature advection (Carlson 1998, p 239). When this thickness minimum is placed over the surface cyclone no more baroclinic amplifying takes place and the cyclone will

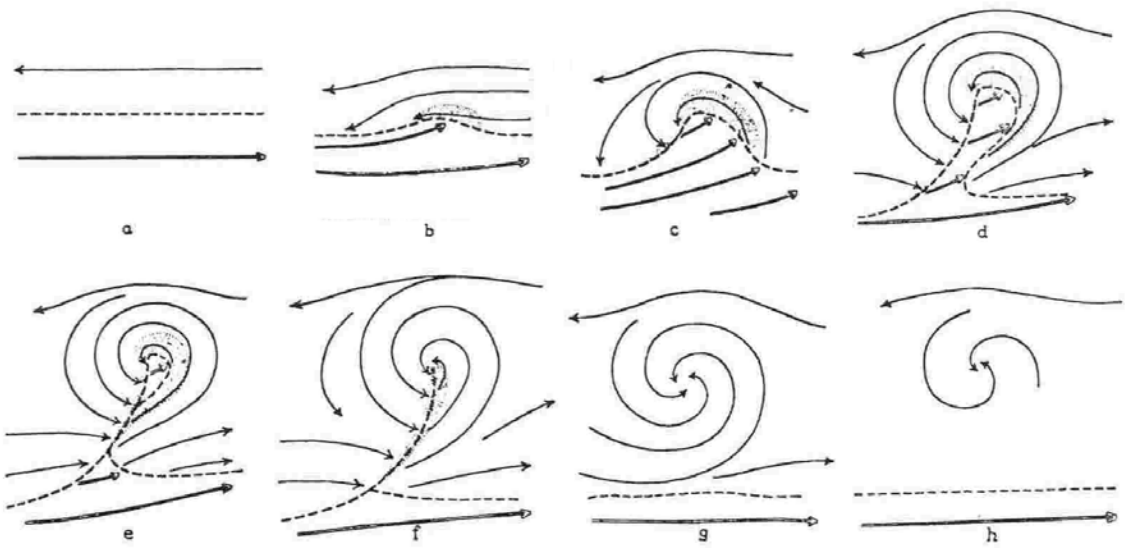

Fig. 2.4: Vertical view of events on low altitudes in cyclonic development. Solid lines are airflow and dashed line is frontal boundaries. The stages are: (a-b) incipient disturbance, (c-d) rapid development, (e-f) maturity and (g-h) decay. (From Bjerknes and Solberg (1926))

diminish by time due to friction, internal dissipation and barotropic transfer into kinetic energy on other scales (Carlson,1998, p 233). The Norwegian model is closely connected to the baroclinic theory with an infinitesimal disturbance that amplifies. It should though be mentioned, that it seems to be more likely for a preexisting reasonably large disturbance to cause cyclogenesis than for an infinitesimal disturbance.

If the forcing from any of the terms in Eq. 2.13 and 2.14 are strong enough, cyclogenesis may occur although the ideal baroclinic case is not attained. As described by Karlsson (1988) cyclones can develop model with only either a small amplitude wave disturbance in a strong baroclinic zone according to the Norwegian (type A) or a strong vorticity advection area in height, associated with upper levels troughs or jet streaks (type B). The development of cyclones type B is connected to the vorticity advection terms in the omega- and geopotential tendency equation, and may occur in connection with jet streaks or on the west side of a upper level trough. Cyclones of type B, without any pre-existing surface frontal zone, can show a very rapid development and can be difficult to forecast, with large damages caused by strong wind and heavy precipitation (Karlsson, 1988). An example is described at Fig. 2.7.

A jet streak is a maximum of the wind speed in the jet stream, located just below the tropopause, with the area of maximum wind speed shaped like a cigar. As the wind speed south and north of the “cigar” is lower than inside, a vorticity minimum is placed on the south boundary of the “cigar” and a maximum on the north side. That implies that positive vorticity is located on the southwest and northeast side of the jet-streak, and negative vorticity advection on the northwest and southeast side as illustrated in Fig. 2.5. Therefore cyclogenesis is likely to occur on the southwest and northeast boundary and anticyclogenesis on the northwest and southeast side (Karlsson 1988).

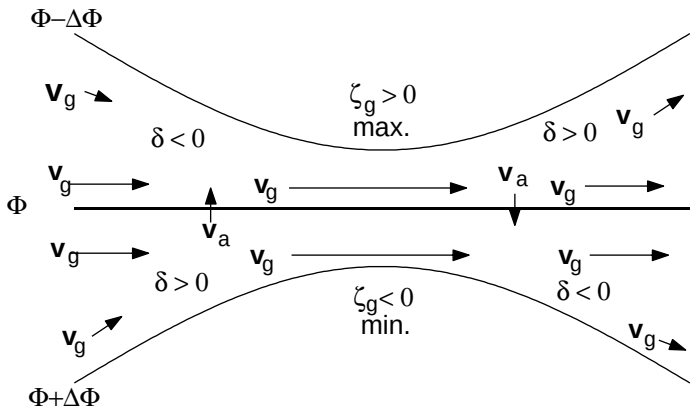

Fig. 2.5: Parcel dynamics in a jet streak. Geopotential heights Φ, geostrophic wind v_g, ageostrophic wind v_a , vorticity ζ_g , convergence $\delta<0$ and divergence $\delta>0$. (Redrawn after Bluestein, 1993).

2.8 Explosive cyclonic development and Polar low

The polar front theories described above applies reasonably well to most cyclones occurring over Scandinavia, but some cyclones show explosive development and are much more rapidly deepening than an ordinary frontal cyclone. The "bomb" is an explosive cyclogenesis occurring most frequently over the ocean in wintertime downstream an upper level trough near the strongest sea-surface gradients. It can have deepening rates of more than 1 hPa/h, which is more than in an ordinary frontal cyclogenesis (Bluestein, 1993, p121). A typical value of deepening rate for a normal cyclone might be about 10 hPa in 24 hours. In Bluestein (1993, p 121) some factors that enhance cyclogenesis and distinguish 'bombs' from a more ordinary cyclogenesis are described:

1. Sensible heat transport between a warm ocean and cold air creates low static stability that enhances the forcing in the omega-equation.
2. Strong temperature gradient at the sea surface enhances temperature advection.
3. Turbulent transfer of water vapor and heat from a sea surface increases when wind increases, and "bombs" may therefore behave like tropical cyclones.
4. Unusually large values of temperature advection at high levels.

The center of a bomb contains air that is warmer than the advancing cold air, but colder than the retreating warm air, in contrast to frontal cyclones with a cold-air center (Bluestein 1993, p 126). Satellite picture of "bombs" are found in Fig. 2.6 and 2.7.

Polar lows appear in the cold air mass, north of or behind the cold front. They are usually quite shallow and of relatively small scale (less than 1000 km) (Carlson, 1998, p 257). They form near strong sea and air temperature gradients. Often occur intense cumulus convection or comma shaped clouds. Polar lows influencing weather in southern Sweden is often formed between Iceland and Great Britain. Polar lows have three features in common (Carlson, 1998, p 257): Firstly they have conditionally unstable lapse rates, i.e. when an air parcel is lifted by e.g. turbulent flow and reaches level of condensation, it

becomes unstable. Secondly they are associated with strong low-level baroclinity, and thirdly, they occur in regions where cold air is advected over a warm surface as e.g. warm water. Convection causes latent heat to release and, due to moist-adiabatic temperature decrease, the temperature in convection cells will be higher creating a baroclinic environment that enhances the cyclogenesis. Fig. 2.8 shows a satellite picture of a polar low.

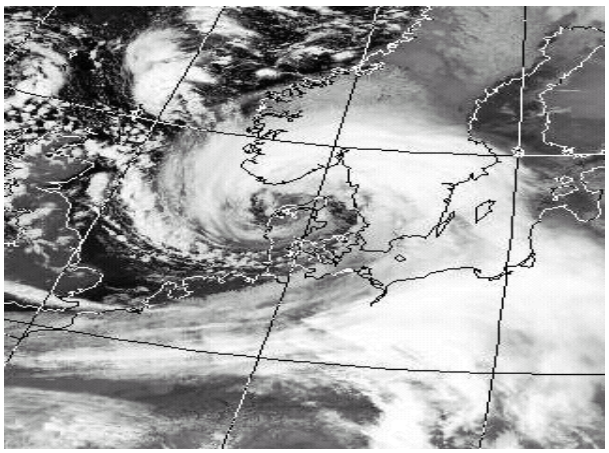

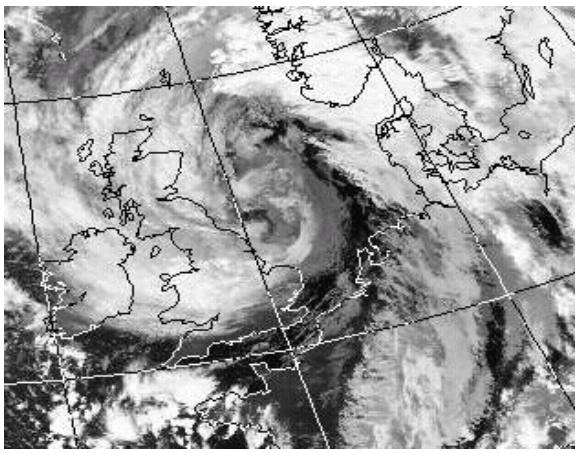

Fig. 2.6 (left) and 2.7 (right): NOAA channel 4 satellite pictures from two storms both showing very rapid 'bomb-like' development. Left: The 'storm of the century' over Denmark at 16.25 on the 3:rd of December 1999. Right: Satellite picture from the 16:th of October 1987 at 08.18. British forecasters rejected the occurrence of this destructive cyclone only a couple of hours before it hit the British west coast. Pictures from Dundee Satellite Receiving Station, Dundee University, Scotland. http://www.sat.dundee.ac.uk/

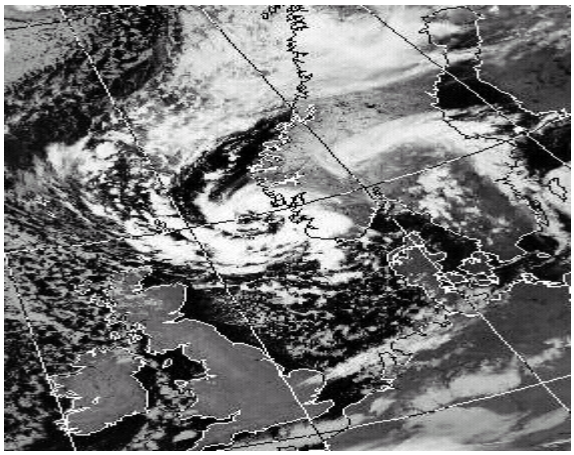

Left: Fig. 2.8: Satellite picture from NOAA channel 4 of a polar low west of Norway on the 16:th of October 1993 at 05.11. Picture from Dundee Satellite Receiving Station, Dundee University, Scotland. http://www.sat.dundee.ac.uk/

2.9 Cyclogenesis and climate change

Many climate models show an increase in overall global temperature with the same patterns influencing baroclinic activity (Harvey, 2000, p 226):

- A greater mean annual warming at the surface and in the lower troposphere at high latitudes than at low latitudes.
- A greater warming in the winter than in the summer at high latitudes, particularly over the ocean surface
- A greater overall warming of the land surface than of the ocean surface
- A greater warming of the upper troposphere in the tropics than at middle and high latitudes
- A decrease in the tropical lapse rate due to greater warming in the upper troposphere than in the lower troposphere and at the surface
- An increase in the polar lapse rate due to greater warming in the lower troposphere than in the upper troposphere

As the low level temperature increases more at high latitudes than at low latitudes, the low level temperature gradient weakens. The opposite occurs in the upper levels where the temperature gradient increases, causing stronger upper level winds. The low level gradient weakening decreases baroclinity and the increased wind speeds at high levels enhances baroclinic development. Further more, changes in the lapse rate affects the static stability parameter, a higher lapse rate gives lower static stability and increased vertical motion, which enhances baroclinic development. The net effect of these factors needs to be quantified to determine whether cyclogenesis is enhanced or not.

Although the global average low-level temperature gradient weakens, regional gradients may increase. This might be the case if only a slight warming occurs over e.g. Greenland and a greater warming occurs over Europe. The preexisting temperature gradient enhances and cyclogenesis is enhanced. As seen in the introduction, the output from different climate models differs when it comes to cyclogenesis, although the change of temperature shows similar patterns.

3. Data

Both reanalyzed data for mean sea level pressure from actual occasions and model data were used for the frequency and pressure pattern analysis. These data were provided by the MICE-project. A geostrophic wind series calculated from measurements was, together with measurements of mean winds, used to verify that the geostrophic wind calculated from gridded pressure data is a useful parameter to find occasions associated with hard winds.

3.1 Reanalyzed NCEP-data for mean sea level pressure

Reanalyzed daily data of mean sea level pressure data from NCEP (National Centers for Environmental Prediction) for the period from 1961-01-01 to 1990-12-31 covering the area latitude 30° N-75° N and longitude 15° W - 45° E with a latitudinal and longitudinal spacing of 2.5° provided by the MICE-project were used to analyze historical storm situations. The data were interpolated with cubic splines to the same grid that is used for HadAM3H data, with horizontal spacing of 1.87° and a vertical spacing of 1.25° for the MICE area. The NCEP/NCAR reanalysis project is described more extensively in Kanay et al. (1996).

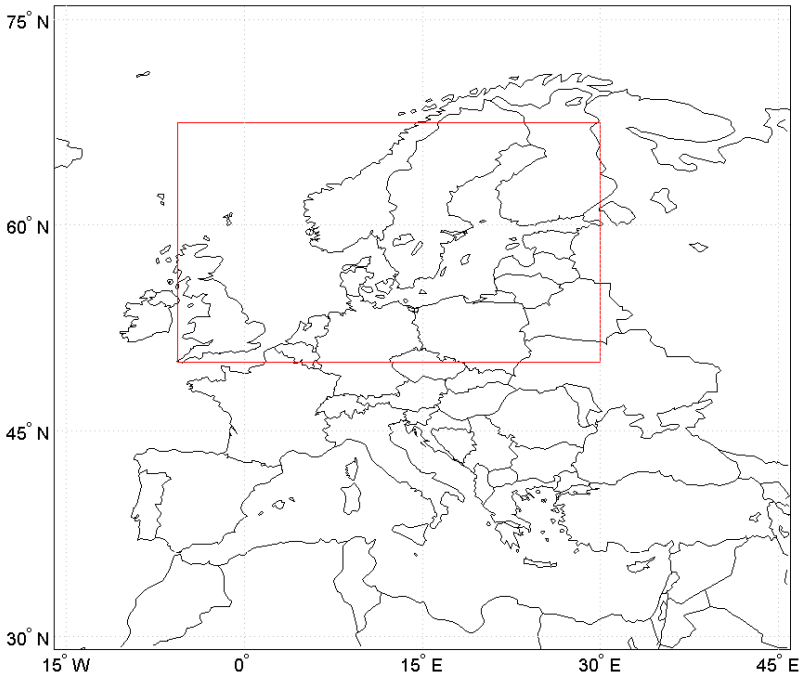

Fig. 3.1: MICE area and in the rectangle the area used for PCA and cluster analysis.

3.2 Model data from HadAM3H and HadRM3

Two different outputs from the model HadAM3H developed at United Kingdom Meteorological Office, 'Met Office' or UKMO, in Bracknell, were used. The HadAM3H model is a global atmospheric model, which takes its boundary conditions from the atmospheric-ocean coupled circulation model HadCM3 but uses a higher spatial

resolution than HadCM3. Information of the HadAM3H model is found in Pope et al. (2000). The HadAM3COM run ((2) in Fig. 3.2), code *'acdhd',* uses boundary conditions from the HadCM3COM run, codes *'aaxzl', 'aaxzx'* and *'aaxzz'* ((1) in Fig. 3.2), starting in the period from 1860 to 1989 with observed atmospheric properties and continuing with emission scenario B2 (see Watson et al. (2002)) to 2099. Data from the period 1961-1990 were used. The HadCM3 model was then again started from 1990 with atmospheric properties according to the Intergovernmental Panel on Climate Change (IPCC) emission scenario A2 and run until 2099 ((4) in Fig. 3.2), run cod *'aaxzi'*. The IPCC A2 scenario is a kind of a worst-case emission scenario, with a very heterogeneous world and rather slow and regionally differentiated economic growth, and increased emissions of many green house gases (Watson et al 2002). Data from the model HadAM3H were used for the period 2070-99 and is denoted HadAM3A2 ((5) in Fig. 3.2), code *'acftc'*.

To see how a model with higher spatial resolution treats strong pressure gradients, mean sea level pressure from the regional model HadRM3H runs (3) and (6) (see Fig. 3.2) for the 10 occasions associated with the highest geostrophic winds in each of the HadAM3COM and HadAM3A2 runs are used. As a consequence of the high resolution, this dataset requires a huge amount of memory and calculation capacity. Therefore only few days are extracted. The HadRM3H model uses a polar rotated grid with a grid spacing of 0.44 degrees relative to a pole at 38°N and 190°E.

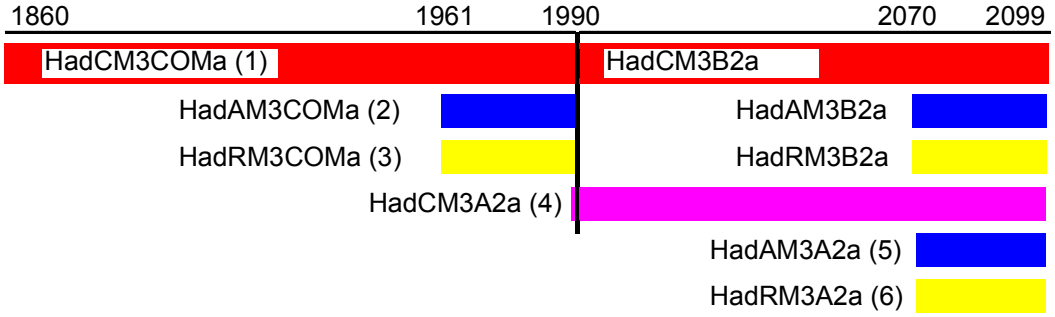

Fig. 3.2: Different runs from Hadley Center used in this report. The dataset from the common period (HadCM3COM and HadAM3COM) is the runs (1) and (2). The A2 run (4) starts with the model value at 1989 and runs with atmospheric values from IPCC scenario A2. The dataset HadAM3A2 refers to (5). The letter 'a' denotes the ensemble. Totally 3 ensemble runs were carried out but only data from the first run is used in this project.

3.3 Geostrophic wind series

A geostrophic wind series with three daily wind values based on sea level pressure measurements at the SYNOP stations in Falsterbo, Göteborg-Säve and Visby was used to compare calculated geostrophic wind based on gridded data with geostrophic wind based on measurements. The wind series based on pressure measurements spanned from 1860 to 2000, and data for the period 1961-01-01 to 1990-12-31 were used. The geostrophic wind for this period is based on pressure measurements at 06, 12 and 18 UTC. The wind

series based on pressure measurements is calculated by Hans Alexandersson, SMHI, and is described in Alexandersson and Vedin (2002).

3.4 Measured wind data

Measurements of 10 m 10 min mean wind at 12 UTC for ground stations in Falsterbo, Kullen, Hanö, Måseskär, Såtenäs and Karlsborg for the period 1961-01-01 to 1990-12-31 and for
Sturup the period 1971-12-01 to 1990-12-31 were used to investigate the relation between geostrophic and measured wind.

3.5 Supplementary information

In the archives available at the excellent web site ‘www.wetterzentrale.de’ reanalyzed data of mean sea level pressure and 850 hPa temperature from NCEP are found. The primary use of these data was to check the procedures to read and plot data from the provided data set and to investigate the development of some of the most severe cyclones during the interesting period.

An unpublished compile of forest damages was provided by Ph. D. student Carin Nilsson at the Dept. of Physical Geography and Ecosystem Analysis, Lund University. Dates with strong winds and severe wind damages are found in the Swedish Meteorological Society at the web site ‘http://www.svemet.org/orkantab3.htm’, reprinted in Appendix 1.

A couple of Matlab programs and functions were developed and used to simplify the work and to ensure the possibility of similar recalculations.

4. Method

4.1 Calculating Geostrophic Winds

A program to calculate geostrophic wind from gridded pressure data was developed. The program calculates the direction and magnitude of the geostrophic wind in a new grid point (U) in the middle of four pressure grid points (p) shown in Fig. 4.1.The gradient in each new grid point is calculated as the mean value of a centered space finite difference scheme using the value in the 4 surrounding grid points. That gives a pressure gradient approximation with an accuracy of 2nd order.

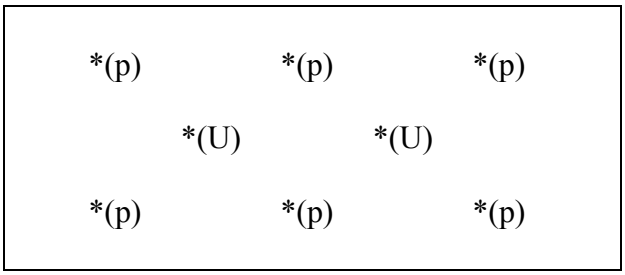

Fig. 4.1: Structure of grid points, pressure marked (p) and geostrophic wind marked (U)

NCEP-data was transformed into grid points used by the HadAM3H model by cubic spline interpolation. The geostrophic wind for each grid point, geographically placed as shown in the map at Fig. 4.2, was calculated. An example of geostrophic wind and pressure field is found in Fig. 4.3.

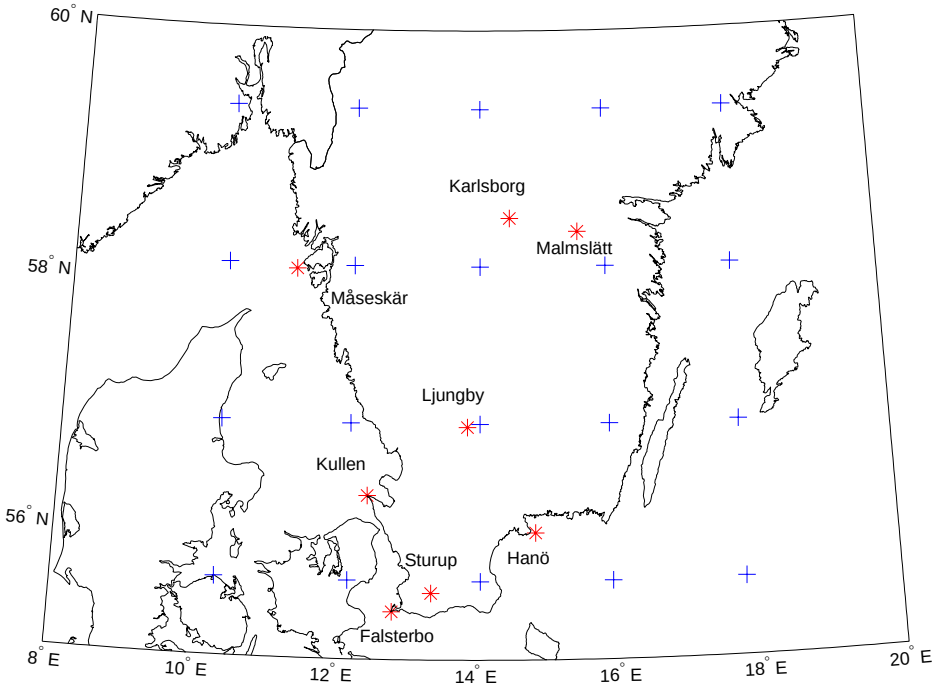

Fig. 4.2: Geographic location of wind grid points (+) *and ground measurement stations* (∗) *used above.*

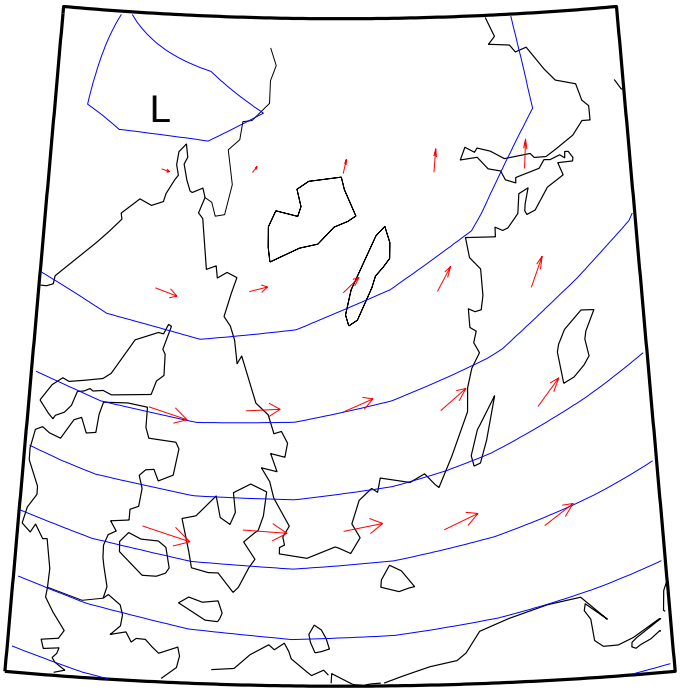

Fig. 4.3: Illustration of geostrophic wind and NCEP pressure field, data for1981-11-24.

To validate if geostrophic wind is a useful tool to determine high values of real wind, the geostrophic wind calculated from interpolated NCEP-data was first compared to a geostrophic wind calculated by Hans Alexandersson, SMHI, using data of pressure measurements on ground stations at Falsterbo, Gothenburg and Visby. Secondly, geostrophic wind calculated from interpolated NCEP-data at a certain grid point was compared to averages of 10 min measurements of 10 m wind on ground stations close to the actual grid point.

4.2 Analog method

The use of the analog method is applied in many different feature, at least six different areas of use can be identified, e.g. short range forecasts, specification of surface weather, long-range forecasting, estimation of atmospheric predictability, estimations of the dimensions of the phase spaces and cluster analysis (van den Dool, 1994). Perhaps the most well known examples of use in the analog method are the German 'Grosswetterlagen' (Gerstengarbe et al., 1999) and the 'Lamb Weather Types' for the British Isles, where all days' weather between 1861 to February 1997 has been classified (see e.g. http://www.cru.uea.ac.uk/cru/data/lwt.htm). The topic of using analogs is described in detail by Lorenz (1969), used in e.g. Luksch and von Storch (1998) for estimating heat transport, compared to other methods in Zorita and von Storch (1999) and used for downscaling surface air temperatures in Timbal and McAveney (2001). The two states that resemble each other most closely are analogues. The analogue is in Zorita and von Storch (1999) defined by the pattern that minimizes the distance

$$\sum_{k=1}^{n}\left[z_k - x_k(t)\right]^2 \qquad (4.1)$$

where z is the reference state in the pool of states and x is the measurement value. In this project the correlation and the distance in Eq. 4.2 were used to find analog situations.

In many analog applications, the topic is to determine parameters that are poorly described in a course resolution model. Sufficiently similar occasions in a pool of previous occasions are searched. The value of the searched parameter is then assumed to be similar to the parameter value observed in the analogue. Van den Dool (1994) showed that the library must be very large to employ good forecasts on a daily timescale. However, in this case focus is not on the forecasting skill so larger errors can be accepted in searching analogs. Applied here, the wind speed is the searched parameter and the analogues are based on pressure patterns.

Two different pools of possible analogues were used. In the first, the database of possible analogues is based on 29 different occasions with measured storm winds and documented wind caused forest damages. The second uses a pool of 432 occasions with a geostrophic wind exceeding 25 m/s. This means, for the first case, that although the calculated geostrophic wind does not reach the strength of a storm situation, a certain pressure field may be associated to local hard winds and work as an analogue to a future storm situation. A similar approach to find a pressure pattern associated to wind erosion in Southern Sweden is performed by Ekström et al. (2002).

4.3 Methods to find storm days in model data

4.3.1 Method 2: Using analog pressure field

Two different approaches were used to find occasions with high likeliness of forest damages. In the first days when the wind caused severe damages on forests and environment were identified. In a summary by the Swedish Meteorological Society (reprinted in Appendix 2) dates with strong and damaging storms are found. These were used to verify that the forest damages were caused by the wind and not by heavy snow or other parameters. The days with great forest damages were checked with reanalyzed NCEP-data on ‘www.wetterzentrale.de’ and in the dataset provided by the MICE-project. If the observed strong winds were associated with an obvious cyclone or, at least strong pressure gradients and therefore high geostrophic winds, these situations were regarded as significant situations associated with large damages on forests. Dates of interest are found in Tab. 4.1. In Tab. 5.2 the calculated geostrophic wind for each storm day is shown. As seen, although most days are associated with real strong geostrophic winds, not all days are. Although some pressure fields do not give high geostrophic winds over southern Sweden, they are associated to a situation that in reality caused damaging winds. It might be cyclones that moves over the geographic area of interest between two sampling times, or cyclones that disappear.

The pressure fields for the 29 stormy days were clustered into sufficiently many clusters. Empirically it appeared that at least 15 different clusters were proper to be used for covering sufficiently many different storm occasions. Thereafter different ways to find analog situations to the storm situations in both the HadAM3COM dataset and the HadAM3A2 dataset were tested. Two methods were applied; one using different threshold values of correlation between each day in model data and the different cluster situations and one using a threshold value of maximum distance calculated from:

$$D^{tu} = \sqrt{\sum_{ij} \left(\left(Y_{ij}^{t} - \overline{Y^{t}} \right) - \left(X_{ij}^{u} - \overline{X^{u}} \right) \right)^{2}} \qquad (4.2)$$

Here D^{tu} is the sum of the distances between all grid points of the pressure field at occasions t and the cluster u, Y^{t}_{ij} is the current pressure value in the grid point (i,j), Y^{t} is the mean value of the pressure on current occasion, and X denotes the values of the cluster. Compared to Eq. 4.1 this measure of distance is better to find similar circulation patterns, but does not pay attention to mean pressure differences. As neither the correlation is concerned of mean pressure value, the classification into clusters is only based on circulation patterns and not on absolute pressure.

It turned out that the best method to find analog situations was to combine the distance value and the correlation. To find analogues a threshold value for the correlation larger than 0.94 and a total distance lower than 70 hPa on totally 300 grid points between the current day and the closest cluster were used.

Tab. 4.1: Data with destructive storms over southern Sweden

1964-12-13	1973-11-19	1976-01-05	1981-11-24	1986-01-20
1967-10-17	1973-11-23	1978-09-11	1983-01-18	1988-11-29
1968-01-10	1975-01-04	1978-12-30	1983-10-19	1988-12-30
1969-03-09	1975-12-06	1980-04-18	1983-12-30	1990-01-26
1969-09-22	1975-12-08	1981-02-08	1984-01-13	1990-02-26
1969-11-01	1975-12-23	1981-11-21	1985-11-06	

4.3.2 Method 2: Using geostrophic wind

The other attempt was based purely on geostrophic wind. As seen in Tab. 5.2 most days have geostrophic winds exceeding 25 m/s. Therefore 25 m/s was chosen as a threshold value and dates with a geostrophic wind exceeding 25 m/s were picked out. Some of these days were checked with observations of storm wind (winds exceeding 21 m/s) on Swedish ground stations in Väder och Vatten (1975-1990). Most occasions with strong geostrophic winds were associated with stormy days (45 of 49 counted on geostrophic wind > 27m/s based on wind calculations in pressure grid points which in general gives lower geostrophic values and larger errors than the one described previously).

Principal Component Analysis, explained in Appendix 1, was applied to NCEP-data for the 432 days with geostrophic wind exceeding 25 m/s to reduce the amount of data and to

filter out noise. The explanation of total variance contained in each PC is shown in Fig. 4.3 (left). The ten first PC:s are plotted in Appendix 5. The first 30 PC:s were picked out to reduce the amount of data. These 30 PC:s include all components that participate with more than 1.35% in any storm occasion (Fig. 4.4).

Unrotated PCA based on the covariance matrix was used. The covariance field was assumed to contain more information than the correlation field. Two different applications of PCA were used; as a data reduction method and for a comparison between the main PC:s of different climate scenarios. Rotated PCA may be proposed for the second use, but in this case the use of the pressure map was to see if the PCA and their corresponding eigenvalues look similar in different scenarios, not to investigate their physical interpretation.

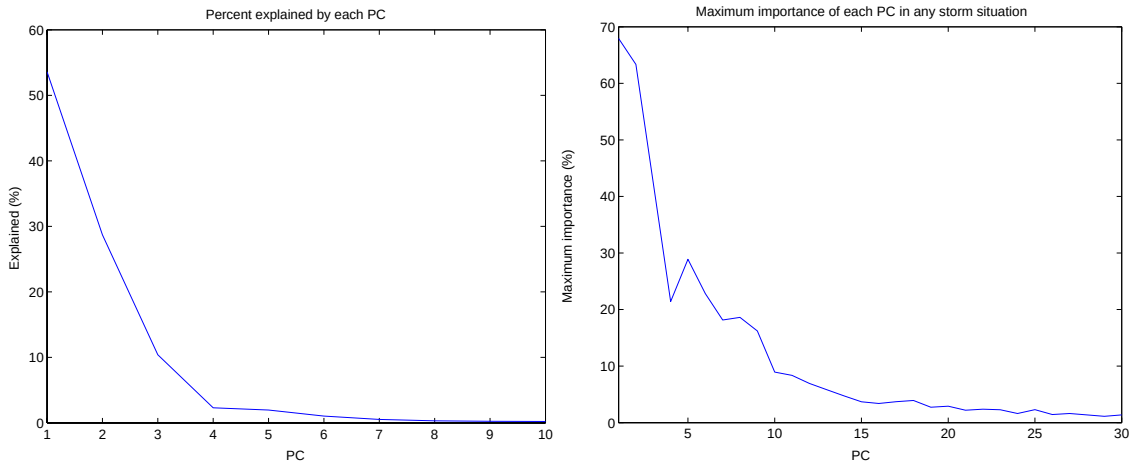

Fig. 4.4: (Left) Total variance contained in each PC and (right) maximum importance of each PC based on days with geostrophic winds exceeding 25 m/s in NCEP data.

To find a reasonable number of storm groups the filtered data was divided into 10 different clusters, using the Matlab function '*clusterdata*'. The function uses 'Euclidian distance' calculate the distance between each object, and then a nearest-neighbor clustering algorithm was used. The mean value of mean sea level pressure in each cluster is plotted in Appendix 4. The distance between each cluster is found in the dendrogram in Fig. 4.5. Making cluster analyses to data that were filtered through PCA turned out to be more successful in creating usable clusters than cluster analysis on raw data.

To find analog situations in HadAM3COM and HadAM3A2 situations with geostrophic wind exceeding 25 m/s were searched. The PC:s of these situations were calculated, and the main eigenmodes compared. If the pressure patterns at stormy occasions tend to change between two runs, it is likely that either the eigenmodes or their connected eigenvalues will change. If both the eigenmodes and the eigenvalues are conserved it is reasonable to believe that no or little change of the pressure pattern will occur.

A program was developed that uses both the correlation and the distance in Eq. 4.2 between each situation and cluster to find which of the clusters that show most similarities to that certain occasion. If the correlation or distance is closer to any cluster

than a certain threshold value, it will be classified as a day belonging to that cluster. A change in the pressure field at stormy days might give a change in the frequency of each cluster classification. A threshold value for the correlation was set to 0.70 and for the distance to 160. Occasions that did not fulfill the threshold values were then clustered using a minimum Euclidian distance algorithm to find main patterns in pressure distribution.

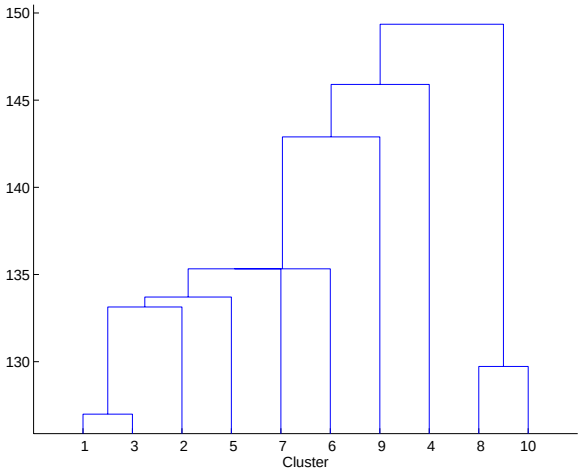

Fig. 4.5: Dendrogram where the y -axes shows the minimum distance between each cluster.

4.4 Evolution of cyclones

If the frequency of storms and their associated pressure patterns change it is likely that changes in the strength and geographical position of strong cyclogenesis occur. A method was tested to investigate possible changes of cyclogenesis and the changes in the frequency distribution between polar- and frontal lows. The idea was to find occasions in HadAM3COM and HadAM3A2 with correlation over a threshold value to a chosen mean value of a cluster based on NCEP data. For each occasion the days before are compared and clustered. The frequency of each cluster and their pressure patterns was then thought to be useful tool to compare geographic location and strength of cyclogenesis.

Unfortunately this attempt requires a temporal resolution of data that is much higher than what was provided by the available data. There is no possibility to, with sufficient accuracy, determine the origin or path of a cyclone with 24 h between each observation. In many cases, it is not even possible to determine if a certain cyclone is present on the map the day before, if it is new developed or if it is a moving old cyclone.

A cyclonic development study would require a higher spatial resolution and a wider area of investigation, including the strong baroclinic zones over the west Atlantic. A more complete cyclonic development investigation would require data of 500 hPa geopotential and stream patterns and 850 hPa temperature, as well as sea level pressure.

5. Results

First the results from the comparison between calculated geostrophic wind from NCEP data and geostrophic wind from measured pressure as well as from the result of the comparison with measured wind are presented. Then results from the two different methods to find storm situations in the HadAM3H model are found. Finally the results from a comparison with the calculated wind from a high-resolution regional model are found.

5.1 Geostrophic wind

The calculated geostrophic wind based on NCEP data that are interpolated and transformed into HadAM3H-grid is compared to calculated geostrophic wind for the triangle Falsterbo-Gothenburg-Visby based on ground station measurements at the triangle corners. Correlation between NCEP-geostrophic wind and measurement based wind for each calculated grid point for different pressure observations is shown in Tab. 5.1. Values for the grid point (56.875° N , 14.065° E), close to Ljungby (marked in Fig. 4.2), were used to make monthly and a total comparison of wind speeds. Total and monthly plots and statistical parameters for a comparison of these data are found in Appendix 1, Fig. A1. The slope of the regression line is 0.88 and the correlation coefficient 0.82. NCEP-data give in general slightly higher winds, but at most extreme events measured pressure based winds gives higher values. The spatial resolution in NCEP-data is better than in the measurements, but the resolution in time is worse in NCEP-data and some extreme events may be filtered out during the initialization.

The regression line is determined with the Matlab function *'robustfit'* that uses a weighted least square iteration method that is less sensitive to outliers than the ordinary least square method. As seen the confidence interval for the regression parameters is rather small due to many observations. Each month contains between 847 and 930 observations, and the total number of observations is 10957. The 95 % prediction interval is mainly large, around 13 m/s totally.

Observes 10m 10-minute mean-wind for some ground stations are plotted in Appendix 3, Fig. A3-2, together with calculated geostrophic wind from NCEP-data at the grid point closest to the station. Coastal stations measurements show a closer correlation to geostrophic wind than continental ones and a larger value of the slope of the regression line. Anyway, a clear correlation between geostrophic wind and measurements are seen. The total width of the 95 % prediction interval varies between different places between 7-13 m/s.

A plot of calculated geostrophic winds from NCEP-data for the 432 occasions when the wind exceeds 25 m/s compared to wind from measured pressure data for a grid point near Ljungby is found in Fig. A3-3, left. The correlation between the series in this case is only 0.59 and the slope of the regression line 0.79. A plot between NCEP calculated storm winds at grid point (2,2) and measured wind at Måseskär is found in Fig. A3 right. Here the slope of the regression line is as low as 0.28 and the correlation 0.37.

Tab. 5.1: Correlation between calculated geostrophic wind from NCEP-data and geostrophic wind by Hans Alexandersson SMHI.

Evening the day before					
Lat/Lon	**10.315**	**12.190**	**14.065**	**15.940**	**17.815**
59.375	0.376	0.457	0.506	0.534	0.547
58.125	0.410	0.479	0.554	0.605	0.622
56.875	0.488	0.539	0.595	0.644	0.664
55.625	0.502	0.542	0.579	0.619	0.643
Morning					
Lat/Lon	**10.315**	**12.190**	**14.065**	**15.940**	**17.815**
59.375	0.517	0.600	0.624	0.631	0.601
58.125	0.583	0.676	0.750	0.766	0.720
56.875	0.678	0.757	0.819	0.837	0.793
55.625	0.652	0.712	0.758	0.779	0.759
12 z					
Lat/Lon	**10.315**	**12.190**	**14.065**	**15.940**	**17.815**
59.375	0.591	0.644	0.636	0.617	0.567
58.125	0.649	0.720	0.760	0.741	0.669
56.875	0.725	0.791	0.827	0.811	0.740
55.625	0.690	0.744	0.776	0.772	0.725
Evening					
Lat/Lon	**10.315**	**12.190**	**14.065**	**15.940**	**17.815**
59.375	0.590	0.601	0.569	0.544	0.495
58.125	0.629	0.662	0.670	0.635	0.564
56.875	0.686	0.719	0.722	0.686	0.615
55.625	0.654	0.683	0.688	0.663	0.609
Next morning					
Lat/Lon	**10.315**	**12.190**	**14.065**	**15.940**	**17.815**
59.375	0.402	0.385	0.367	0.363	0.339
58.125	0.415	0.413	0.415	0.403	0.370
56.875	0.468	0.463	0.450	0.429	0.395
55.625	0.468	0.462	0.445	0.424	0.397

In Tab. 5.2 the maximum calculated geostrophic wind speeds and direction in any of the twenty grid points derived from NCEP-data are shown together with geostrophic wind

speed and direction based on pressure measurements for the 29 days with observed severe wind caused damages.

Tab. 5.2: Geostrophic wind at morning, lunchtime and evening, calculated by Hans Alexandersson, SMHI, and maximum geostrophic wind in any of the wind grid points calculated by NCEP-reanalyzed data. The direction in degrees is from where the wind blows, using the definition of angle from the unit circle.

Year	Month	Day	Morn.	Dir.	12z	Dir.	Noon	Dir.	NCEP	Dir.
1964	**12**	**14**	19.8	150	14.8	176	12.3	177	22.1	178
1967	**10**	**17**	15.1	315	15.5	228	20.7	214	19.9	8
1968	**1**	**11**	43.5	8	36.8	20	27.6	29	22.8	22
1969	**3**	**9**	30.8	107	24.5	106	13.5	110	30.7	159
1969	**9**	**22**	29.9	216	39.5	172	32.3	140	29.2	171
1969	**11**	**1**	15.9	168	23.3	190	30.0	149	25.1	160
1973	**11**	**19**	27.8	214	27.3	198	7.7	11	28.8	177
1973	**11**	**23**	29.3	139	20.6	140	15.2	148	28.4	162
1975	**1**	**4**	27.5	173	28.0	137	25.4	133	28.1	155
1975	**12**	**6**	24.1	98	19.4	106	18.2	110	29.3	138
1975	**12**	**8**	22.8	110	23.5	107	15.7	129	28.1	136
1975	**12**	**23**	22.6	154	19.2	160	20.4	173	22.6	166
1976	**1**	**5**	38.0	222	18.8	239	25.4	93	23.2	166
1978	**9**	**11**	13.7	164	13.2	219	23.5	133	19.6	169
1978	**12**	**30**	21.1	4	22.7	2	24.3	356	27.9	352
1980	**4**	**18**	25.4	123	32.4	114	31.9	104	41.9	143
1981	**2**	**8**	24.7	187	37.1	167	31.5	122	28.8	160
1981	**11**	**21**	34.6	141	33.8	136	21.4	134	32.9	158
1981	**11**	**24**	46.1	202	49.3	206	36.0	181	46.3	171
1983	**1**	**19**	27.0	196	32.4	159	31.8	116	43.3	161
1983	**10**	**19**	28.2	183	33.9	183	31.0	161	29.9	169
1983	**12**	**30**	21.2	192	29.1	167	33.3	147	25.4	165
1984	**1**	**13**	28.2	219	44.1	232	65.3	215	29.7	216
1985	**11**	**6**	45.3	213	42.1	208	33.5	180	36.9	176
1986	**1**	**20**	14.9	93	9.8	165	14.4	199	17.0	150
1988	**11**	**29**	9.5	35	31.4	77	23.8	88	26.4	137
1988	**12**	**30**	15.8	177	21.5	168	27.8	144	19.2	163
1990	**1**	**26**	36.9	205	43.1	201	29.6	170	34.4	191
1990	**2**	**27**	31.9	163	26.4	161	24.3	159	33.4	182

5.2 Method 1

Correlation and the distance defined in Eq. 4.2 were calculated between all occasions sampled in HadAM3COM as well as HadAM3A2 model and a clustered data with 15 pressure patterns based on 29 real storm occasions described in Ch. 2. The HadAM3COM run gave 206 occasions that fulfilled the threshold values compared to 205 occasions from the HadAM3A2 run. Only 15 respective 12 of those occasions were associated with geostrophic winds lower than 15 m/s, which is the lowest maximum

value in any cluster. The frequency of occasions divided into each cluster is found in Tab. 5.3.

Tab. 5.3: Frequency of days in each model with correlation > 0.94 and Distance < 75 to any cluster. Vmin is lowest maximum wind of any day and Vmean mean wind of all days. Corr and dist refers to the assignment to clusters of each method for each day.

HadAM3COM				**HadAM3A2**		
Days	206			**Days**	205	
Vmin	12.9			**Vmin**	12.0	
Vmean	22.5			**Vmean**	21.9	
Cluster	**Corr**	**Dist**		**Cluster**	**Corr**	**Dist**
1	65	64		**1**	67	62
2	0	0		**2**	0	0
3	0	0		**3**	0	0
4	7	5		**4**	3	0
5	6	0		**5**	2	0
6	0	0		**6**	1	1
7	2	1		**7**	9	5
8	0	0		**8**	0	0
9	0	1		**9**	0	0
10	102	104		**10**	95	99
11	0	0		**11**	0	0
12	7	2		**12**	9	3
13	0	7		**13**	0	10
14	12	17		**14**	13	19
15	5	5		**15**	6	6

The total frequency of days close enough to the predefined clusters is almost conserved between the two model runs, although some differences may occur in the frequency of each cluster. As seen in Appendix 6 cluster number 4, 9 and 12 are quite similar and may be regarded as similar types. The total frequency of these three groups is almost unchanged. Furthermore cluster 5 and 7 show similar pressure patterns and their total frequency is almost conserved. As seen in the Tab. 5.3 no significant changes in occasions similar to those associated to damaging winds during the period 1961-1990 are seen between the HadAM3COM run and HadAM3A2 run.

5.3 Method 2

5.3.1 HadAM3COM

The geostrophic wind for each wind grid point was calculated from the HadAM3COM run. The frequency of storm winds is shown in Tab. 5.4. There are 644 occasions with geostrophic wind greater than 25 m/s. Overall this dataset tends to give higher geostrophic winds than NCEP-data. Occasions with winds greater than 25 m/s were

Tab. 5.4: Occasions with winds exceeding 20, 25, 30, 35 and 40 m/s, maximum winds and mean wind for the period 1961-01-01 to 1990-12-31.

	20 m/s	25 m/s	30 m/s	35 m/s	40 m/s	45 m/s	Maximum winds (m/s)			Mean
NCEPHad	1314	432	94	25	5	2	46.3	45.5	43.3	13.3
HadAM3COM	1863	644	200	56	18	7	54.4	50.1	48.8	15
HadAM3A2	1830	597	191	51	10	3	77.3	58.6	56.3	14.9

picked out and PCA was applied. The rate of explanation and maximum importance for each PC is found in Fig. 5.1. The ten most important PC:s are found in Appendix 5. Those PC:s were compared to the main PC:s from NCEP data. If there are any big differences in pressure pattern of stormy days, either the importance or the principal component itself should differ between the datasets. The three first PC:s are similar, giving that most of the information is equal. PC 4-6 show small differences in the center, but show mostly the same variance field. The really big differences occur first at PC 8, which consists only 0.3 % of the total variance (Tab. 5.5). It is not probable that the observed differences in the first 7 PC:s may change the gradients or storm patterns, they do not occur where the strongest gradients in the PC:s are found.

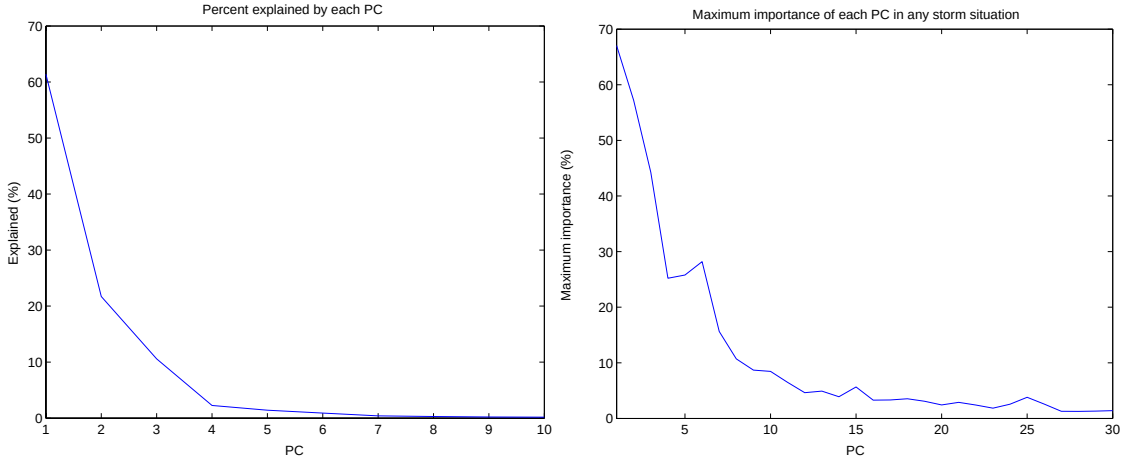

Fig. 5.1: HadAM3COM PC, total importance and maximum importance

The correlation and a distance algorithm described in Eq. 4.2 were used to associate classify each situation into the clusters based on real storms in NCEP. The frequency distribution and mean value of each cluster are found in Tab. 5.6. Both methods of classifying seem to give similar results. Those occasions that differ either classify to different but similar clusters or are not closely related to any cluster. A picture of mean pressure value for the storm occasions is found in Appendix 5 after the PC:s. Occasions that did not fulfill the threshold value of 0.70 for the minimum correlation (Tab. 5.6, 'no class') was divided into 10 new cluster using a Euclidian distance algorithm. Most of these occasions (67 out of 83) were associated with easterly geostrophic winds due to a high over northern Scandinavia, 6 occasions were associated to southerly geostrophic winds and a high over Russia. Plots of the most frequent clusters are found in Appendix 7.

Tab. 5.5: Total importance in % of each PC in NCEP, HadAM3COM and HadAM3A2

PC	NCEP	COM	A2
1	53.6	61.4	61.2
2	28.7	21.7	22.4
3	10.4	10.6	10.3
4	2.3	2.3	2.2
5	2.0	1.4	1.3
6	1.0	0.9	0.8
7	0.5	0.4	0.4
8	0.3	0.3	0.3
9	0.3	0.2	0.2
10	0.2	0.2	0.2

5.3.1 HadAM3A2

The same procedure was applied to HadAM3A2 data. The frequency of storm occasions is found in Tab. 5.3. Storm days were picked out and PCA was applied. The first 8 PC:s look significantly similar to the 8 first PC in HadAM3COM data in a visual comparison. The total variance contained in the first PC:s is shown in Tab. 5.3. and are similar in the HadAM3COM and HadAM3A2 runs. When most PC:s as well as their relative importance are rather equal in both simulations and the mean value is almost the same, the functions that contain the most information of the variance are the same, the real pressure patterns in storm occasions seem to be unchanged.

The stormy days were divided according to the NCEP-based clusters. The frequency of each cluster is found in Tab. 5.6 and the mean value of the correlation and the distance for the days classified into each cluster are found in Tab. 5.7.

The occasions that did not meet the requirement of a correlation of 0.70 were divided into 10 clusters. 23 of 81 days was associated to a high over Russia and southerly winds, 47 with a low somewhere over the North Sea, Denmark, Southern Sweden or the southern Baltic Sea (Appendix 7).

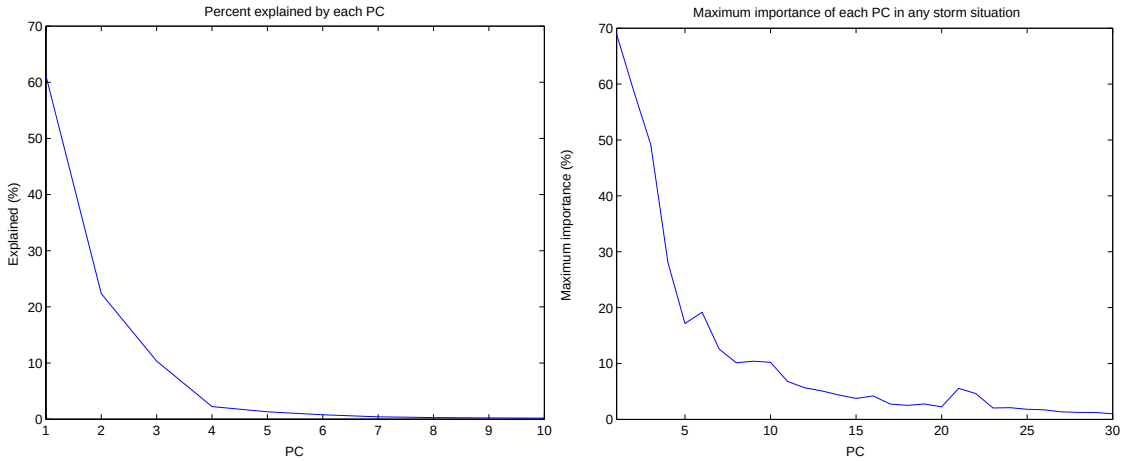

Fig. 5.2: HadAM3A2 PC, total importance and maximum importance

Tab. 5.6: Frequency distribution of occasions with winds greater than 25 m/s. COM refers to HadAM3COM and A2 to HadAM3A2

NCEP	NCEP		COM	Dist	COM	Corr	A2	Dist	A2	Corr
Cluster	Freq.	%	Freq.	%	Freq.	%	Freq.	%	Freq.	%
1	421	97.7	96	14.9	65	10.1	72	12.1	66	11.1
2	1	0.2	21	3.3	18	2.8	20	3.4	20	3.4
3	1	0.2	4	0.6	27	4.2	2	0.3	21	3.5
4	1	0.2	20	3.1	16	2.5	18	3.0	6	1.0
5	1	0.2	82	12.7	122	18.9	59	9.9	81	13.6
6	1	0.2	85	13.2	113	17.5	103	17.3	135	22.6
7	2	0.5	7	1.1	10	1.6	11	1.8	9	1.5
8	2	0.5	70	10.9	47	7.3	66	11.1	46	7.7
9	1	0.2	135	21.0	130	20.2	125	20.9	118	19.8
10	1	0.2	27	4.2	13	2.0	26	4.4	14	2.3
No class			97	15.1	83	12.9	95	15.9	81	13.6
Total	431		644		644		597		597	

Tab. 5.7: Mean correlation and distance for the occasions classified into each cluster.

	A2	A2	COM	COM
	Meancorr	MeanDist	Meancorr	MeanDist
1	0.89	119	0.88	113.2
2	0.86	121	0.86	124.7
3	0.86	151	0.88	139.1
4	0.81	130	0.81	121.7
5	0.92	110	0.92	111.1
6	0.84	119	0.83	124.4
7	0.91	89	0.84	101.0
8	0.90	104	0.91	110.5
9	0.84	118	0.82	123.9
10	0.91	108	0.90	117.8

5.4 Comparison between geostrophic winds in the HadAM3H and HadRM3H models

Pressure data for 10 occasions with highest calculated wind speed in the COM and A2 runs were extracted from a very large dataset of mean sea level pressure from the HadRM-model for the same scenarios. The geostrophic wind speed was calculated from RM-data was compared to the previous calculated wind geostrophic wind speed. The maximum wind speed for each day is found in Tab. 5.8.

Tab. 5.8: Geostrophic wind speed in any wind grid point in the two models HadAM3H and HadRM3H for the runs COM and A2. Wind speed for the 10 windiest days in the HadAM3COM and HadAM3A2 run.

	AM3COM	RM3COM			AM3A2	RM3A2
1	54.4	26.0		**1**	77.3	23.6
2	46.4	28.6		**2**	58.6	34.1
3	45.1	22.4		**3**	56.3	31.6
4	44.7	39.3		**4**	44.0	9.3
5	43.7	39.1		**5**	43.4	41.9
6	43.2	22.0		**6**	41.2	20.2
7	41.8	29.4		**7**	40.8	35.2
8	38.7	32.3		**8**	39.7	46.0
9	38.7	35.1		**9**	39.6	34.1
10	38.5	19.8		**10**	39.4	37.3

6. Discussion and conclusions

6.1 Geostrophic winds

The comparison of calculated geostrophic wind from interpolated NCEP-data and from the measurements of pressure at three ground stations shows a satisfying correlation of 0.83 (Tab. A3-1) and a value of the regression line close to 1. Also measurements show a correlation between 0.63 and 0.76 as seen in Tab. A3-2, which implies a close connection between calculated geostrophic winds and measured winds. Measurements tend to be a little lower, as seen in Fig. A3-2 and Tab. A3-2. Due to boundary layer effects this is expected. The reasonably high correlation between geostrophic and measured winds gives that the possibility for high winds and associated damages on forests, environment and community is dependent on the geostrophic wind. Therefore the geostrophic wind can be used as a tool to determine the likely occasions of stormy days. However, it should be noted that this method might miss those situations where a high geostrophic wind passes over the area of interest so fast that the temporal resolution of the data set is too low to reproduce the storm occasion. The relation between geostrophic value and true horizontal velocity is within 10-15% for large-scale motions according to Holton (1992, p 40). A reduction value of about 20% at coastal stations for strong cyclones was used by Alexandersson and Vedin (2002).

At the calculated storm occasions in NCEP-data, both the 'measured pressure'-based method and the wind measurements do not show such a close relation to wind NCEP-wind as in the total case. First it should be noted that the 432 storm occasions determined from the calculated wind from NCEP-data are based on the maximum value in any of the wind grid points. Therefore, some days are not associated with high wind speeds at all at these points and the wind peak may occur at another time of the day than the time used here. Second, the correlation might be expected to decrease at high wind speeds, due to stronger influence of e.g. friction and turbulence. Wind speeds are measured at 12 UTC, the maximum value of each day may show a better correlation to calculations.

From the 95 % prediction interval in Fig. A3-2 it can be seen that a geostrophic wind of 25 m/s gives, for inland station such as Sturup, a measured wind between around 8 and 16 m/s of measured 10 m 10 min mean wind. In Talkkari et al. (2000) a measured 10 m mean wind value of 16 m/s was used for forest damages, although it was noted that lower values might give damages. From this it can be concluded that a geostrophic wind of 25 m/s might cause damages on forests, although most wind observations at occasions with 25 m/s geostrophic wind does not exceed Talkkari's threshold value for forest damages. It is likely to believe that trees are more vulnerable to maximum winds than to mean winds. Furthermore wind gusts may cause fatigue of trees, although the mean wind speed is not reaching a certain threshold value. Gustiness and maximum winds are dependent on local effects and are very hard to resolve in a high-resolution model as well. Here it is assumed that the probability of strong maximum winds and strong gusts due to synoptic scale weather systems are functions of the geostrophic wind speed, i.e. that the likeliness for strong gusts increases with increased geostrophic wind.

6.2 The frequency of strong wind speeds and associated pressure pattern

In the review of the impact of a climate change on cyclogenesis in Ch. 2.9 it was concluded that many climate models show a greater warming over continental areas and at high latitudes, and a greater warming in the upper troposphere in the tropics than at higher latitudes. The ground temperature increase is most prominent in wintertime in those areas that today are the coldest. That may affect e.g. the large wintertime high-pressure area over northern Russia. If the temperature increases most at northerly latitudes, the average temperature gradient weakens. As the available potential energy is dependent on the temperature gradient, weaker gradients mean less APE[1], although the absolute energy of the atmosphere is increased. On the other hand the increase in upper level temperature gradient increase APE and the high level winds, which enhance cyclogenesis. Furthermore, warmer air contains more water vapor, and condensation heat released in sectors of rising air may enhance baroclinic development. A qualitative conclusion would be that there will be enhanced possibilities for cyclogenesis of 'type B', described in Ch. 2.7, and reduced possibilities for development of 'type A'. The total effect has to be quantified in circulation models. As described in Ch. 1 many models show an increased frequency of storms in the North Sea and Baltic Sea area in a future climate change, so even an analysis of the HadRM3H winds seen in Fig. 6.1.

The attempt to find analog situations by searching for occasions in HadAM3COM and HadAM3A2 gave almost the same results for both runs. The result of this method is that the frequency of situations causing damaging strong winds during the period 1961-1990 seems to be almost unchanged, and no real changes in the extreme situations of wind climate is likely to occur. The analog method assumes that the relations between parameters are conserved if two situations are similar enough, and no attention is paid to the possibility of the relation of meteorological parameters to change in a changed climate. This problem is discussed for downscaling situations in Zorita and von Storch (1999). Moreover, only 29 occasions of destructive winds were used and the data used contains of a daily observation at a fixed time, not necessarily at the time of the most extreme event. Therefore, the pressure pattern at the most intense instant of the weather phenomena may not be resolved in the pressure data used, the pressure pattern clustered may show a 'weaker' weather event than what really caused the winds. The analogs that are searched will then be closely related to this 'weaker ' weather and not necessarily to the extreme event. When only pressure pattern are used to find analog situations no information is available about the development. Hence only parameters significantly related to sea level pressure at the resolved time can be searched. Searching for analogs that show the same development requires much more data, but could be used to estimate extremes that occur between each resolved time step.

The frequency of occasions with geostrophic wind with a magnitude over 25 m/s on any of the wind grid points is slightly greater for the control period described by the HadAM3COM-model than the simulated future-scenario by the HadAM3A2 model (644 compared to 597 occasions from Tab. 5.3). In contrast, interpolated and reanalyzed

[1] The anticipated temperature increase means an increase of the absolute energy of the atmosphere. As usual in physics it is only the energy that is convertible into work that we notice.

NCEP-data, gives only 432 occasions with winds over 25 m/s. The lower frequency in NCEP data may be explained by the initial poorer spatial resolution, the interpolated data may not resolve local high-pressure gradients as well as an initially closer gridded dataset. On the other hand, the closer gridded HadRM3H-data does not give as high wind as HadAM3H model on the extreme events in HadAM3H, as discussed later.

Some of the clusters in Appendix 4 are likely to present same type of weather systems, but at different geographic locations. Cluster number 2, 3 and 4, called group A, might be regarded as a moving isolated low and are therefore analyzed as one group. Cluster no. 1, 5, 7, 8 and 10 (group B) are associated with a trough or low over northern Scandinavia and is analyzed as on group. Cluster 6 and 9 are regarded as different groups, although the correlation and distance algorithm had a tendency to regard these days as quite similar. The frequency of each group is found in Tab. 6.1.

The clusters formed by the days that did not fulfill the correlation threshold value were a bit different in the two runs. In the COM-run 67 of 83 days that were not clustered were associated with easterly geostrophic winds and a high over northern Scandinavia. Six occasions were associated to southerly winds and a high over Russia. The group similar to the first almost disappeared in the HadAM3A2 run, and the second increased to 23 of 81 occasions. In the frequency Tab. 6.1 it is seen that frequency of cluster number 6 that also is associated with easterly flow is increased in the A2 run, but together with the unclassified occasions a decrease in days with high easterly geostrophic winds are seen. This decrease might be connected to the expected weakening of the wintertime Russian high.

Easterly storm days, caused by a high-pressure area placed north of a low, are seldom observed, but their impact on environment may be severe. Usually no or little precipitation occurs in the easterlies, and under dry conditions, fresh breeze and stronger winds can cause large wind erosion with great impact on agriculture areas (Ekström et al., 2002). The relatively low frequency of easterly storm days may inhibit the environment to protect itself from easterly winds. Therefore, the probability for damages and impacts on the environment caused by wind may be greater for an easterly wind than for an equally strong westerly wind. This can be seen in e.g. Nilsson (2003) where only a few storm occasions from NNE caused more severe damages than an the much more common NW storms.

In Tab. 6.1 it is seen that the frequency of group A defined above is slightly decreased, but its relative frequency remains. For group B the frequency tends to decrease significantly both using the distance or correlation algorithm. As written before a stronger temperature increase at northerly latitudes than at more southerly latitudes tend to move the polar front northward and an increase in the frequency of low passages would increase. On the other hand might the weaker temperature gradients cause decreased cyclogenesis and a decrease in passages of low-pressure systems.

The frequency of the group number 9 in Appendix 4 is slightly decreased. This case is hard to categorize to either group A or B. The low that appears over Scotland has a lot of

future tracks to choose, and it is impossible to determine the track from only a mean sea level pressure map.

Tab. 6.1: The frequency distribution of each group of cluster

	COM Dist	COM Corr	A2 Dist	A2 Corr
Group A	45	61	40	57
Group B	282	257	234	216
6	85	113	103	135
9	135	130	125	118

Two occasions in the HadAM3A2 dataset showed a very unphysical pressure pattern with a lot of short waves and extremely high geostrophic winds (over 55 m/s). These two days where not excluded from the dataset.

A comparison of principal components shows some differences between days in NCEP and HadAM3COM with a geostrophic wind exceeding 25 m/s. No significant changes in PC:s could be observed between the HadAM3COM and HadAM3A2 run. The circulation pattern at windy occasions is mostly conserved. If the total frequency of extreme winds is decreasing, but the relative frequency of each circulation pattern is conserved, no changes in the PC:s are likely to be observed. The small difference in relative frequency described above may not be resolved by principal components.

The two main methods that are used give somewhat different results. Using 29 previous storm occasions as analogues no changes in either frequency or pressure distribution could be detected. The second attempt, gave a slight decrease in total storm occasions, especially for group B and for easterly strong winds. The question is; which of those results is most reliable? The first attempt searching for analog situations may use data not only significant for storm situations and using clusters not covering all possible storm situations, with the result that not all storm situations in the test data are found, and the found analog situations do not exclusively cause storm winds. If it is assumed that the only wind related parameter that determines the rate of damages on forests is the wind speed, the attempt of using geostrophic values is likely to be better. The correlation between strong geostrophic winds and measured high velocities is shown to be satisfying and most of the 29 storm occasions used to define the analogue clusters in the first method were associated with strong geostrophic winds. In this project as many as 644 days of 10800 turned out to be storm days in the HadAM3COM run, or about 20 days a year. This is a little bit more than the storm days observed presented in Alexandersson and Vedin (2002). Maybe a higher threshold value for the geostrophic wind speed might represent storm days more accurately.

6.3 Comparison with a regional model

The geostrophic wind speed calculated from mean sea level pressure data from the HadRM3H model seems to be slightly lower than those calculated from HadAM3H. Here the ten days with the highest gradients in each of the HadAM3H runs are compared to the same days in the HadRM3COM and HadRM3A2 runs. Maybe if all days were included, the situation may look different. Probably higher resolution will give higher geostrophic

winds in average, but maybe not always. Unfortunately the dataset that contains HadRM3H-data is very large and it is not possible to use all data as in the case of the HadAM3H-model. Therefore only few occasions have been checked and no general conclusions can be made whether this model tends to give higher or lower geostrophic wind speeds.

A comparison of the maximum winds in the COM and A2 scenario in the HadRM3H area is done by PD Dr. U. Ulbrich and Dr G. Leckebusch, University of Cologne. The frequency of storm days (maximum wind exceeding 21 m/s) in the COM-run and a comparison with the frequency in the A2 run are found in Fig. 6.1. As no storm days is observed over southern Sweden, no change is possible to observe. In the North Sea and Baltic Sea there seem to be an increase in the storm frequency. This result contradicts the result in this report. The model uses a paramtrization for the wind that takes the e.g. the roughness of the ground, the stabilty paramaters and the topography into account. Although the wind calculation method in the circulation model is more sophisticated than the geostrophic wind method it is not obvious that it is a better estimation of the real wind. This question need to be further investigated.

6.4 Conclusions and outlook

As described in Ch. 1 an increase in storminess over the North sea and Baltic sea is seen in many simulations of the future climate. Here a slight decrease in total storminess is seen, most prominent for easterly high winds. The question is still there; will there be more storm damages in Southern Sweden the next century? Unfortunately, as seen here, different models and methods give different results. This report proposes a probable decrease of winds that will be damaging to forests in Southern Sweden.

As different results are achieved using geostrophic wind as done here and using the wind data achieved from HadRM3H as done in Fig. 6.1, a comparison of these methods would be of great importance. From this report it can be concluded that HadAM3COM gives slightly higher geostrophic winds than the reanalyzed NCEP-data. If the maximum mean wind from the HadAM3COM run does not reach the values of the maximum value of measured 10 m 10 min mean wind, it is probable that the model restrain the occurrence of extreme winds. If that is the case, geostrophic wind might be a better parameter than the wind from the model to determine the likeliness of extreme winds.

As more factors that determine the vulnerability of trees to wind through damages is deeper investigated, more parameters can be taken into account to determine a possible change of vulnerability. Parameters as precipitation in combination with strong winds, wind gusts and freezing days can be incorporated in an analysis to achieve more reliable information.

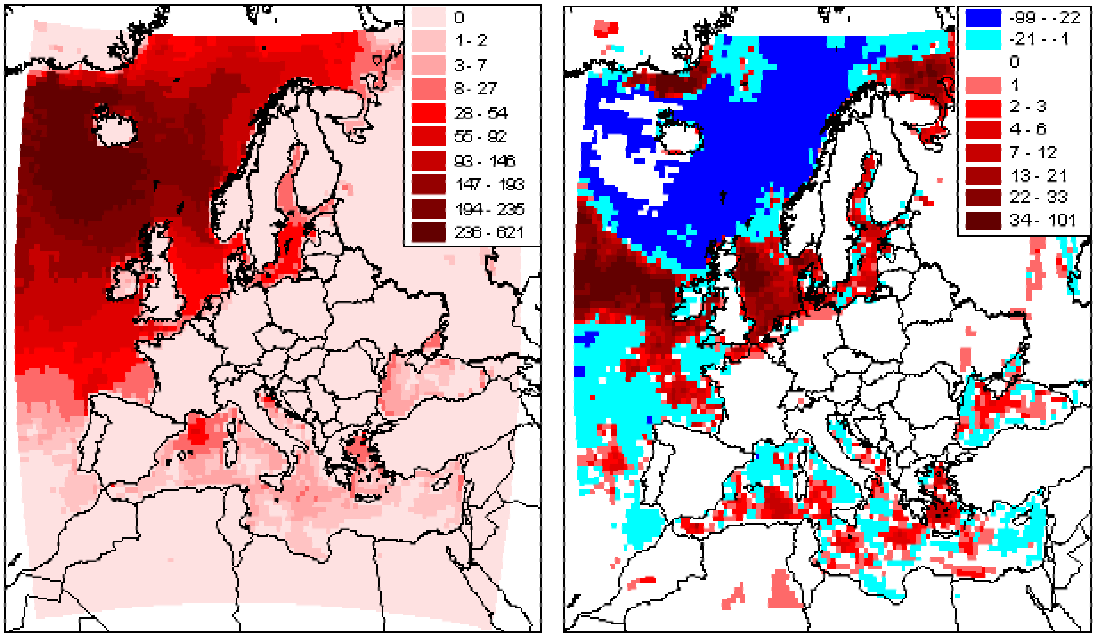

Fig. 6.1: Left: Number of days in the regional HadRM3COM run with winds exceeding 21 m/s. Right: Change of days between the control run and the A2 scenario. Figures provided by PD Dr. U. Ulbrich and Dr G. Leckebusch, University of Cologne.

Acknowledgement

This is a diploma work that terminates my studies in physics and meteorology performed in cooperation between the Dept. of Physics at Lund University and the Dept. of Geophysics at Copenhagen University.

This work was done in association with the European project MICE contract no. EVK2OCT2001-0018.

First I would like to thank my tutor Lars Bärring at the Dept. of Physical Geography and Ecosystems Analysis at Lund University for the work to find an interesting project and the time he has used to make it possible for me to perform this work. Further I would like to thank Carl-Erik Magnusson at the Dept. of Physics, Lund University and Aksel Walløe Hansen at the Dept of Geophysics at NBIfAFG, Copenhagen University, for viewpoints and support. Finally I would like to thank the personnel at the Institute for Physical Geography and Ecosystems Analysis for help and support, especially Carin Nilsson for helping me to get on well on the department and for help to find storm occasions between 1961 and 1990.

The photo on the cover page shows the wind throw damages in Skrylle, about 10 km from the city of Lund, after the storm that is seen on the satellite picture. The storm was one of the most severe in southern Sweden during the late 20:th century. The satellite picture is taken 03.46 UTC on the 4:th of December 1999 by NOAA 14. The photography is provided by Peter Schlyter, Dept. of Physical Geography and Quaternary Geology, Stockholm University. Satellite picture received from Dundee Satellite Receiving Station, Dundee University, Scotland, http://www.sat.dundee.ac.uk/

References

Alexandersson H, Schmith T., Iden K. and Toumenvirta H., 1998, *Long-term variations of the storm climate over NW Europe,* The global atmosphere and the ocean system 6, 1-24

Alexandersson H. and Vedin H., 2002, *Stormar det mera nu?,* Väder och Vatten 10, 2002, SMHI

Beersma J., Rider K. M., Komen G. J., Kaas E. And Kharin V .V., 1997, *An analysis of extra-tropical storms in the North Atlantic region as simulate in a control and 2×CO_2 time-slice experiment with a high-resolution atmospheric model*, Tellus, 49A, 347-361

Bjerknes J. and Solberg H., 1922, *Life cycle of cyclones and the polar front theory of atmospheric circulation,* Geofysiske Publikationer, 3, 3-18

Bluestein H.B. 1993, *Synoptic-Dynamic Meteorology in Midlatitudes. Vol 2, Observations and theory of weather systems*, Oxford University Press, New York, 594 pp

Carlson T.N. 1998, *Mid-latitude weather systems,* The American Meteorological Society, Boston

Ekström M., Jönsson P. And Bärring L., 2002, *Synoptic pressure patterns associated with major wind erosion events in southern Sweden (1973-1991),* Climate Research, 23, 51-66

Fraedrich, K. and Rückert B., 1998, *Metric adaption for analog forecasting,* Physica A, 253, 379-393

Franzén L.G., 1990, *The changing frequency of gales on the Swedish west coast and its possible relation to the increased damage to coniferous forests of southern Sweden,* International Journal of Climatology 11, 769-793

Ganelöv P.O., 01 Feb 2002, *Svåra stormar i Sverige sedan 1900*, Svenska Meteorologiska Sällskapet. From the web page: http://www.svemet.org/orkantab3.htm (2003-05-23)

Gerstengarbe F. W., Werner P.C.,1999, *Katalog der Großwetterlagen Europas (1881 - 1998). Nach Paul Hess und Helmuth Brezowsky. 5., verbesserte und ergänzte Auflage,* Potsdam, Offenbach a. M., 138 pp

Grotjahn R., 1993, *Global atmospheric circulations- Observation and theories,* Oxford university Press, New York

Harvey D., 2000, *Global Warming – The Hard Science,* Prentice Hall, 336 pp

Heino R., Brázdil R., Førland E., Toumenvirta H., Alexandersson H., Beniston M., Pfister C., Rebetz M., Rosenhagen G., Rösner S. and Wiberg J., 1999, *Progress in study of climatic extremes in Northern and Central Europe,* Climatic Change 42, 151-181

Holton J. R., 1992, *An Introduction to Dynamic Meteorology*, Academic Press, San Diego, 511 pp

Kalnay E., Kanamitsu M., Kistler R., and others, 1996, *The NCEP/NCAR 40-yaer reanalysis project*, Bull. Amer. Meteor. Soc., 77, 437-471

Karlsson K.G., 1989, *Jetströmmar och cyklogenes,* Polarfront,nr 61, Oct 1989, 14-21.

Knippertz P., Ulbrich U. and Speth P., 2000, *Changing cyclones and surface wind speeds over the North Atlantic and Europe in a transient GHG experiment*, Climate Research, 15, 109-122

Lorenz, E.N. 1969, *Atmospheric predictability as revealed by naturally occurring analogs*, Journal of the Atmospheric Sciences 26, 639-646

Luksch U and von Storch H., 1999, *An empirical approach for estimating macroturbulent heat transport conditional upon the mean state,* Journal of the atmospheric sciences 56, 2070-2080

Nilsson C., Bärring L., Stjernquist I., Jönsson A.M., Schlyter P., and Samuelsson H., 2003, *Recorded damage in Swedish forests 1900-2000*, In preparation

Persson, G., *Årsrapport 2002*, Swedish Regional Climate Modelling Programme (SWECLIM), Norrköping, 32 pp
Available at: http://www.smhi.se/sgn0106/rossby/sweclim/arsrapport.htm (2003-05-23)

Pope V.D., Gallani M.L., Rowntree P.R. and Stratton R.A., 2000, *The impact of new physical parameterizations in the Hadley Center climate model – HadAM3,* Climate Dynamics, 16, 123-146. Also available at http://www.met-office.gov.uk/research/hadleycentre/models/pope00/index (2003-05-23)

Preisendorfer R., 1988, *Principal Component analysis in Meteorology and oceanography,* Elsevier, New York, 425 pp

Hans von Storch F. and Francis W. Zwiers F. W., 1999, *Statistical analysis in climate research*, Cambridge University Press, Cambridge, 484 pp

Talkkari, A., Peltola H., Kellomäki S., Strandman H., 2000, *Integration of component models from tree, stand and regional levels to assess the risk of wind damage on forest margins,* Forest Ecology and Management 135, 303-313

The WASA group, 1998, *Changing waves and storms in the Northeast Atlantic,* Bulletin of the American meteorological society 79, 741-759

Ulbrich U., and Christoph M., 1999, *A shift of the NAO and increasing storm track activity over Europe due to anthropogenic greenhouse gas forcing*, Climate Dynamics, 15, 551-559

Watson, R.T. and The Core Writing Team (Eds.), 2002, *Climate Change 2001: Synthesis Report*, Stand-alone edition, IPCC, Geneva, Switzerland, 34 pp
Available at: http://www.ipcc.ch/pub/un/syreng/spm.pdf (2003-05-23)

Yarnal, B., 1993, *Synoptic climatology in environmental analysis,* Belhaven Press, London, 195 pp

Zorita E. and von Storch H., 1999, *The analog method- a simple statistical downscaling technique: comparison with more complicated methods,* Journal of Climate, 12, 2474-2489

Zorita E., Hughes J.P., Lettemaier D.P., von Storch H., 1995, *Stochastic Characterization of regional circulation pattern for climate model diagnosis and estimation of local precipitation,* Journal of Climate, 8, 1023-1042

Web based resources:

Reanalyzed NCEP-data:
Wetterzentrale (Updated 2003-05-23)
http://www.wetterzentrale.de/topkarten/fsreaeur.html (2003-05-23)

Satellite pictures in Ch. 2.8 and on cover page from:
Dundee Satellite Receiving Station, Dundee University, UK
http://www.sat.dundee.ac.uk (2003-05-23)

Lamb Weather Types:
Climate Research Unit, University of East Anglia, UK (Updated April 2001)
http://www.cru.uea.ac.uk/cru/data/lwt.htm (2003-05-23)

Appendix 1. Principal Component Analysis (PCA)

Principal component analysis is a method to reduce the amount of data and to find the leading covariance pattern. The covariance between the observations X and Y with n observations is given by:

$$c_{ij} = \frac{1}{n}\sum_{i=1}^{n}\left|\left(X_i - \overline{X}\right)\left(Y_i - \overline{Y}\right)\right| \tag{1}$$

The covariance matrix, where the element c_{ij} is the variance between element i and j, is written:

$$c = \begin{pmatrix} c_{ii} & c_{ij} & \dots & c_{in} \\ c_{ji} & c_{jj} & \dots & c_{jn} \\ \dots & \dots & \dots & \dots \\ c_{ni} & c_{nj} & \dots & c_{nn} \end{pmatrix} \tag{2}$$

From this matrix the eigenvalues and their corresponding eigenvectors are determined. If we let the eigenvectors create a new n-dimensional room the above covariance matrix will transform to a matrix that only consist of diagonal elements in the new coordinate system. Eigenvalues are defined as the values λ that with their associated eigenvectors A fulfills Eq. (3):

$$AY_0 = \lambda Y_0 \tag{3}$$

The eigenvalues are determined by calculating the determinant:

$$\det\left(\lambda \cdot I - A\right) = 0 \tag{4}$$

Corresponding eigenvectors are then determined by Eq. (3). The eigenvectors are sorted in descending order of the value of their corresponding eigenvalues, the eigenvector that are associated to the greatest eigenvalue will then be regarded as the first principal component (PC), the second largest as the second PC etc. The relation between each eigenvalue and the sum of all eigenvalue is a measurement of how much of the total information that is included in each principal component. It should though be mentioned, that a certain PC may be more important in a particular situation than is showed by its total importance. As most of the information is found in the first principal components the use of principal component is a way to reduce the amount of data without hardly any loss of information, and the method may work as a noise filter. There are a couple of different routines to perform PCA. An extensive description of the theories and usage of PCA is found in e.g. Preisendorfer (1988). A more qualitative description is found in e.g. von Storch (1999) or Yarnal (1993).

Appendix 2. Severe storms in Sweden since 1960

Svåra stormar i Sverige sedan 1900 *

År	*Datum*		*Kommentar*
1962	20-feb		Nordlig orkan vid Norrlandskusten (16-17 Hamburgorkanen)
1964	13-dec	14-dec	Västlig orkan vid Svealandskusten
1965	05-jan		Nordnordvästlig orkan längs norrlandskusten
1967	17-okt		Västlig orkan, Ölands S G 40m/s, Hanö 38 m/s. (värst sedan julstormen)
1968	10-11 jan		Nordostlig orkan på södra Östersjön, snökaos i sydsverige 51 mm på Öland
1969	09-mar		Västlig orkan i södra Sverige
1969	22-sep		Västlig orkan längs västkusten (värst under 1900 i västsverige)
1969	01-nov		Allahelgona-stormen. Vindbyar på 35 m/s i Stockholm
1971	08-dec		Nordlig orkan vid norrlandskusten, Grundkallen 34 m/s
1973	01-jan		Orkan i norra Norrland med stor förödelse i skog
1973	19-nov	20-nov	Nordvästlig orkan längs Götalands och Svealands kuster
1973	23-nov		Ölands norra udde hade orkan
1975	04-jan	5-6 jan	Västlig orkan längs väst- och sydkusten
1975	29-maj		Nordostlig orkan på södra Östersjön
1975	24-jun		Nordlig storm med orkanbyar på Östersjön
1975	06-dec		Orkan på Östersjön
1975	08-dec		Orkan på Östersjön
1975	23-dec		Orkan på Östersjön
1976	05-jan		Trettondagsstormen, Vinga syd 39 m/s, Harstena syd 35 m/s
1976	17-apr		Nordvästlig orkan i fjällen med snökaos
1978	11-sep		Västlig orkan längs väst- och sydkusten
1978	30-dec	31-dec	Snöstorm med NO 36 m/s vid Hanö
1980	18-apr	19-apr	Orkanartad storm i sydsverige
1981	08-feb		Orkanbyar i Göteborg, väst 40 m/s. Svåra stormskador
1981	14-apr		Orkan på kalfjället och upplandskusten. Söderarm NV 34 m/s
1981	12-jun		Sommarstorm, ONO 28 m/s vid Örskär, 10-30 cm snö i Dalsland
1981	21-nov		Orkan vid Götalands och Svealands kuster
1981	24-nov		Orkan i sydsverige, Kullen väst 37 m/s,Hanö sydväst 34 m/s
1983	18-jan		SV orkan i sydsverige, Sturup vindbyar på 40 m/s, Hanö väst 33 m/s
1983	18-okt	19-okt	Orkanbyar på västkusten, stormflod 115 cm i Göteborg
1983	23-okt	24-okt	Nordvästlig storm med orkanbyar i norra Norrland, stora skogsskador

1983	30-dec		Västnordvästlig orkan på Svealandskusten, stora stormskador
1984	13-jan		”Tjugondedagsstormen”, sydvästlig orkan vid Kullen, Vinga, Landsort
1985	23-jul		”Ölandsstormen” Ölands norra udde 28 m/s
1985	25-okt		”Norbottensorkanen” , Kiruna NV 34 m/s i byarna och Ö-vik 32 m/s
1985	06-nov		Västlig orkan längs västkusten, Vinga 34 m/s
1986	20-jan		Nordnordvästlig orkan vid sydkusten
1987	13-sep		Nordvästlig storm med orkanbyar vid upplandskusten
1988	28-nov		Orkanbyar i Skåne, Sturup 33 m/s
1988	30-dec		Svår storm i Svealand, Landsort NV 31 m/s, trädfällning. I Älvdalen byar på 35 m/s
1989	02-dec		Orkan i norra Norrland, Kiruna vindbyar på 39 m/s
1990	26-jan		Västlig orkan vid Kullen 37 m/s
1990	26-feb	27-feb	Västlig orkan vid Kullen 38 m/s
1991	09-jan		Västlig orkan längs västkusten
1991	29-dec		Tarfalaorkanen, 69 m/s, elavbrott etc
1992	15-jan	16-jan	Nordlig storm med orkanbyar i Norrland och Svealand
1992	27-jul	28-jul	Sommarstorm längs upplandskusten, Singö 122 mm
1992	20-dec		Orkan vid Tarfala, 81 m/s (högst uppmätta vind i Sverige)
1992	26-dec		Orkanbyar i norra Norrland med svåra skador
1993	14-jan		Orkanvindar över södra Östersjön, Jan Heveliuskatastrofen
1993	01-feb		Orkan vid Tarfala, 76 m/s , saltstorm stoppade malmbanan
1994	28-sep		Storm på norra Östersjön, Estoniakatastrofen
1995	17-nov		Svår snöstorm i Götaland, Kullen 27 m/s, Vinga 26 m/s
1996	29-feb		Orkan i mellersta fjällen, Åreskutan 41 m/s
1996	12-okt		Orkanbyar i fjällen, Stekenjokk 31 m/s, Tarfala vindbyar på 53 m/s
1997	14-jan		Sydvästlig orkan i norra fjällen, Tarfala vindbyar på 69 m/s
1997	21-jan		Orkan i mellersta fjällen, Stekenjokk 43 m/s
1997	30-jan	31-jan	Orkanbyar i fjällen, Vietas NV 32 m/s, Bjuröklubb 26 m/s
1997	06-feb	07-feb	Orkanbyar vid Sylarna 34 m/s
1997	08-mar		Västliga orkanbyar i norra fjällen, Tarfala vindbyar på 57 m/s
1997	11-apr	12-apr	Nord 32 m/s vid Örskär, stormbyar över land
1997	14-apr		Hagelbyar och orkanvindar i Dalarna, i Älvdalen 42 m/s i byarna
1997	17-dec		Orkanvindar över norra Norrland, Nikkaluokta 40 m/s i byarna
1998	30-jan		Nordliga orkanbyar vid Upplandskusten. Örskär 30 m/s, byar på 35 m/s
1998	27-feb		Orkanbyar på västkusten, Måseskär 35 m/s
1998	28-okt		Kortvarigt nv-liga orkanbyar längs sydkusten bakom litet intensivt L
1998	01-dec		Orkanbyar i fjällen, 41 m/s
1999	04-feb		Storm (möjl orkanbyar) längs västkusten. Stormbyar över land. Arlanda vindby på 30 m/s vid KF-pass med åska
1999	29-nov		Orkanbyar på västkusten och Svealandskusten (Måseskär 37 m/s, SA 27

			m/s, Landsort 37 m/s (medel 27m/s)
1999	03-dec	04-dec	"Carola-stormen".Orkan/orkanbyar längs sydkusten 33 m/s i medelvind på Hanö (byar 42 m/s). I Danmark upp mot 50 m/s (Värsta på 1900-talet). Svåra strömavbrott, all trafik inställd i södra Sverige.
2000	29-jan	-31jan	Mycket djupt L (946,2 hPa i Krångede, rekord för januari) gav Storm i södra Sverige. Lotsarna i Kungshamn angav 37 m/s i byarna. I norr snöstorm med upp till 32 m/s i byarna i Abisko natten mot 1 februari.
2000	19mar	20mar	Orkan i Lapplandsfjällen. Stekenjokk 37 m/s med byar på 45. Extremt milt med 18,6 i Oskarshamn.
2001	31 okt	1nov	Intensivt L på bana över södra Svealand gav storm på västkusten och natten mot 1 nov Orkanbyar vid Upplandskusten. Söderarm 30 m/s med byar på 37. 15 000 utan ström. Öresundsbron 28 m/s.
2001	15 nov		Intensivt L med fall 18 hpa på 3h rörde sig österut över norra Sverige. På baksidan Orkanbyar på 38 m/s vid Idre fjäll och Bjuröklubb. Stora skogsskador i södra Norrland, norra Svealand. 100 000 utan ström.
2001	29 nov		Djupt L på Norska havet gav Orkanbyar i södra, mellersta fjällen. Sylarna 43 m/s i byarna. Många fjällvägar ofarbara.
2001	12 dec	13 dec	Intensivt L norr om Skandinavien orsakade Orkanbyar i norr. 67 m/s i byarna vid Tarfala. Gav milt väder med +8,8 i Nikkaluokta den 15:e
2002	28jan	29 jan	Djupt L (970 hPa) på bana från Skottland till Åland gav Orkanbyar längs syd- och västkusten. Hanö 30 m/s med byar på 42. Söderam byar på 29 m/s. Värsta trädfällningen i Kronoberg på 30 år pga väta och ingen tjäle. 100 000 utan ström.7 döda i Storbritanninen pga stormen.

Källa: Väder och oväder under 1900-talet (R Iseborg) fram till 1996. Därefter Väder och Vatten (SMHI). De fall har tagits med där vindbyar på minst orkan (33 m/s) har uppmätts eller omnämnts "orkanbyar". Ett stort antal fall med mycket kraftiga vindar i fjällområdet (främst Tarfala) har ägt rum på senare år efter att automatstationer har placerats ut, vilket kan ge en missvisande bild av att stormarna i fjällen ökat under senare år.
Uppdaterad 2002-02-01
Av Peo

**The table is shortened, the period 1900-1960 is excluded.*

From Ganelöv P.O. (2002)
Printed with permission from Peo Ganelöv.

Appendix 3. Verification of calculated geostrophic wind

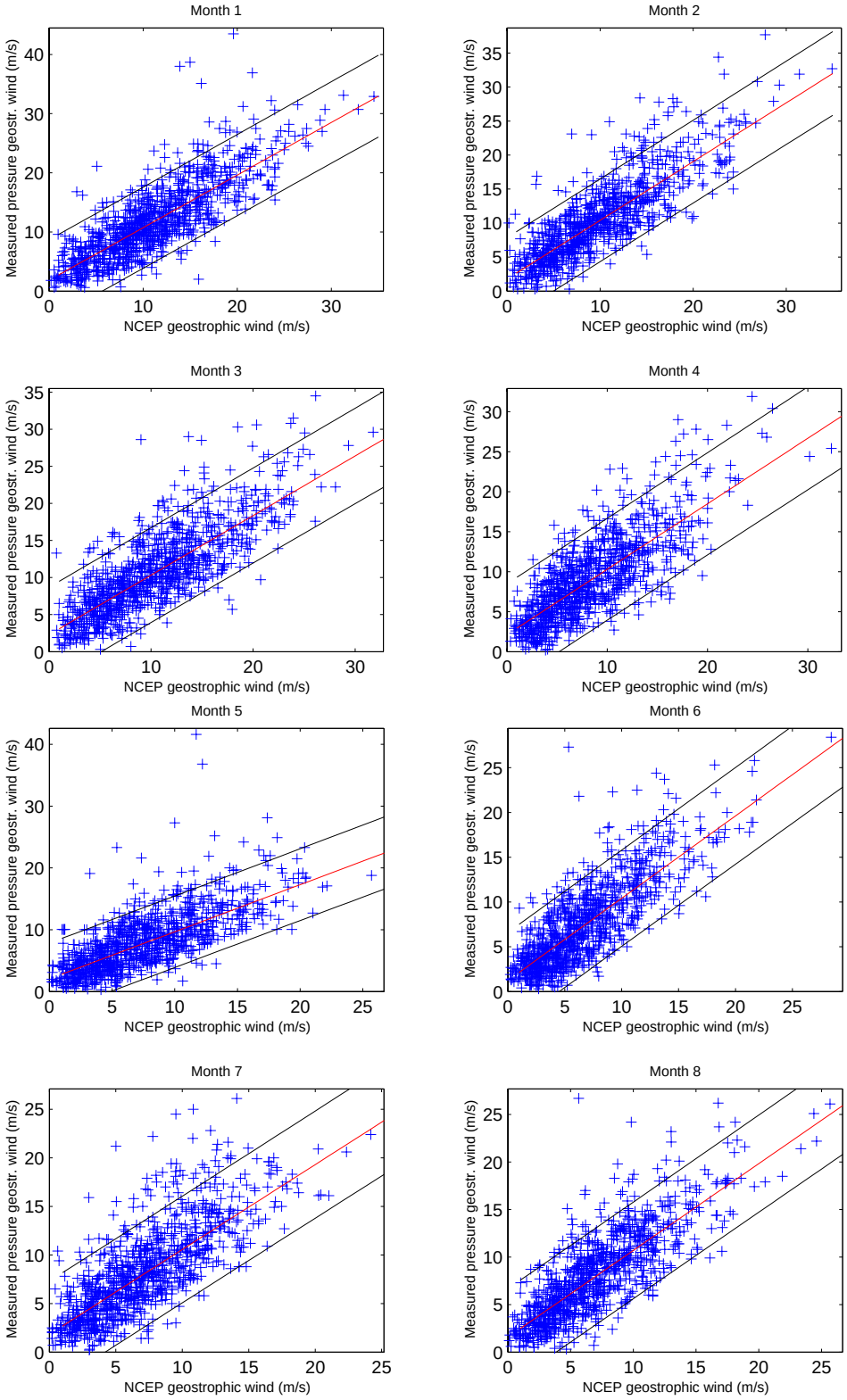

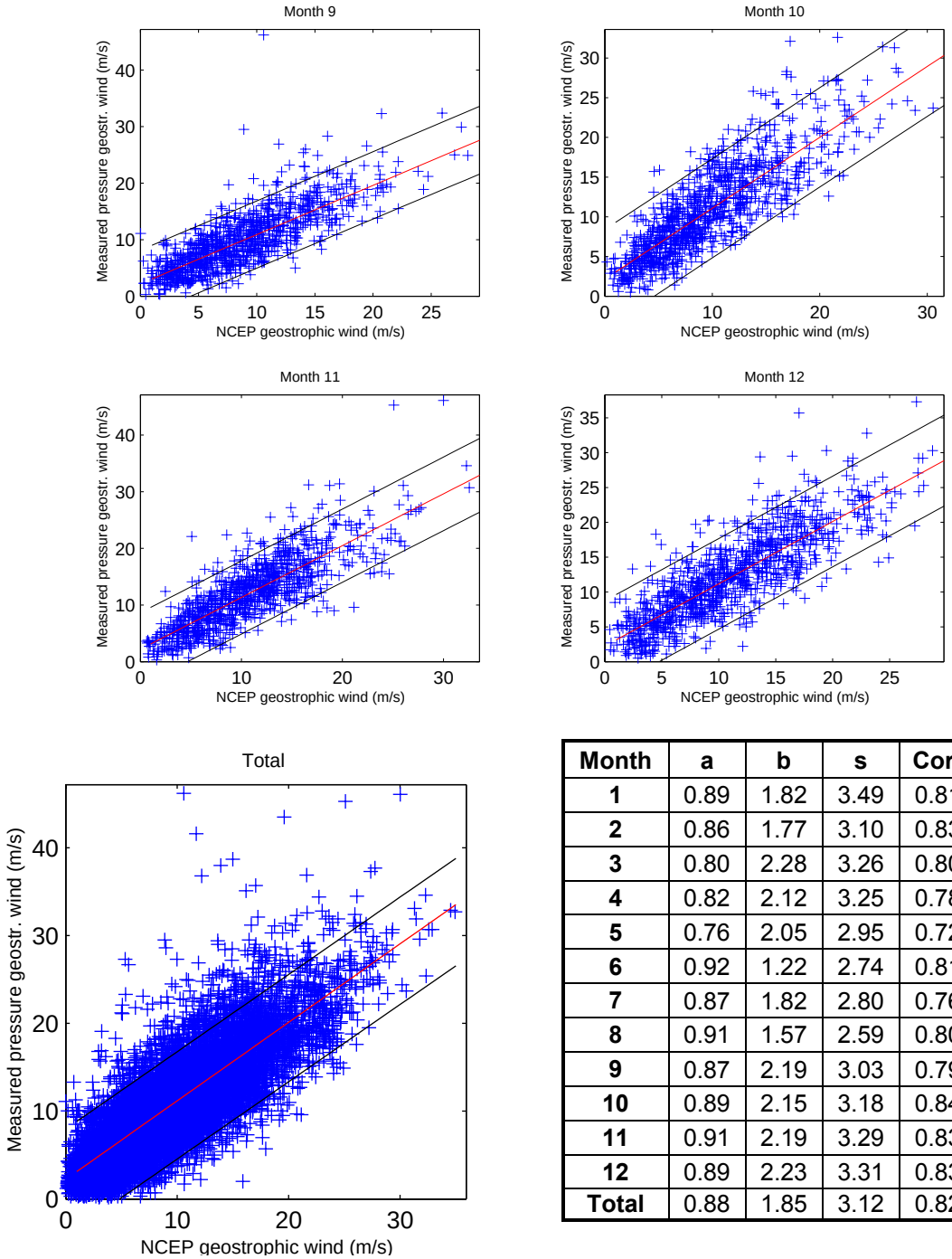

Month	a	b	s	Corr
1	0.89	1.82	3.49	0.81
2	0.86	1.77	3.10	0.83
3	0.80	2.28	3.26	0.80
4	0.82	2.12	3.25	0.78
5	0.76	2.05	2.95	0.72
6	0.92	1.22	2.74	0.81
7	0.87	1.82	2.80	0.76
8	0.91	1.57	2.59	0.80
9	0.87	2.19	3.03	0.79
10	0.89	2.15	3.18	0.84
11	0.91	2.19	3.29	0.83
12	0.89	2.23	3.31	0.83
Total	0.88	1.85	3.12	0.82

Fig. A3-1: Geostrophic wind calculated from interpolated NCEP-data for a grid point at 15.065 ºE and 56.875 ° N plotted with geostrophic wind based on pressure measurements at Falsterbo-Visby-Gothenburg calculated by Hans Alexandersson, SMHI (Alexandersson and Vedin, 2002). Solid lines are regression line(red) and prediction interval (black). The 95% confidence interval of the parameters for the total regression line is a=0.8809±0.0108 and b=1.8458±0.0584.

Tab. A3-1: The coefficients of the regression line (y=ax+b), the measured standard deviation (s) and the correlation between the two different calculations.

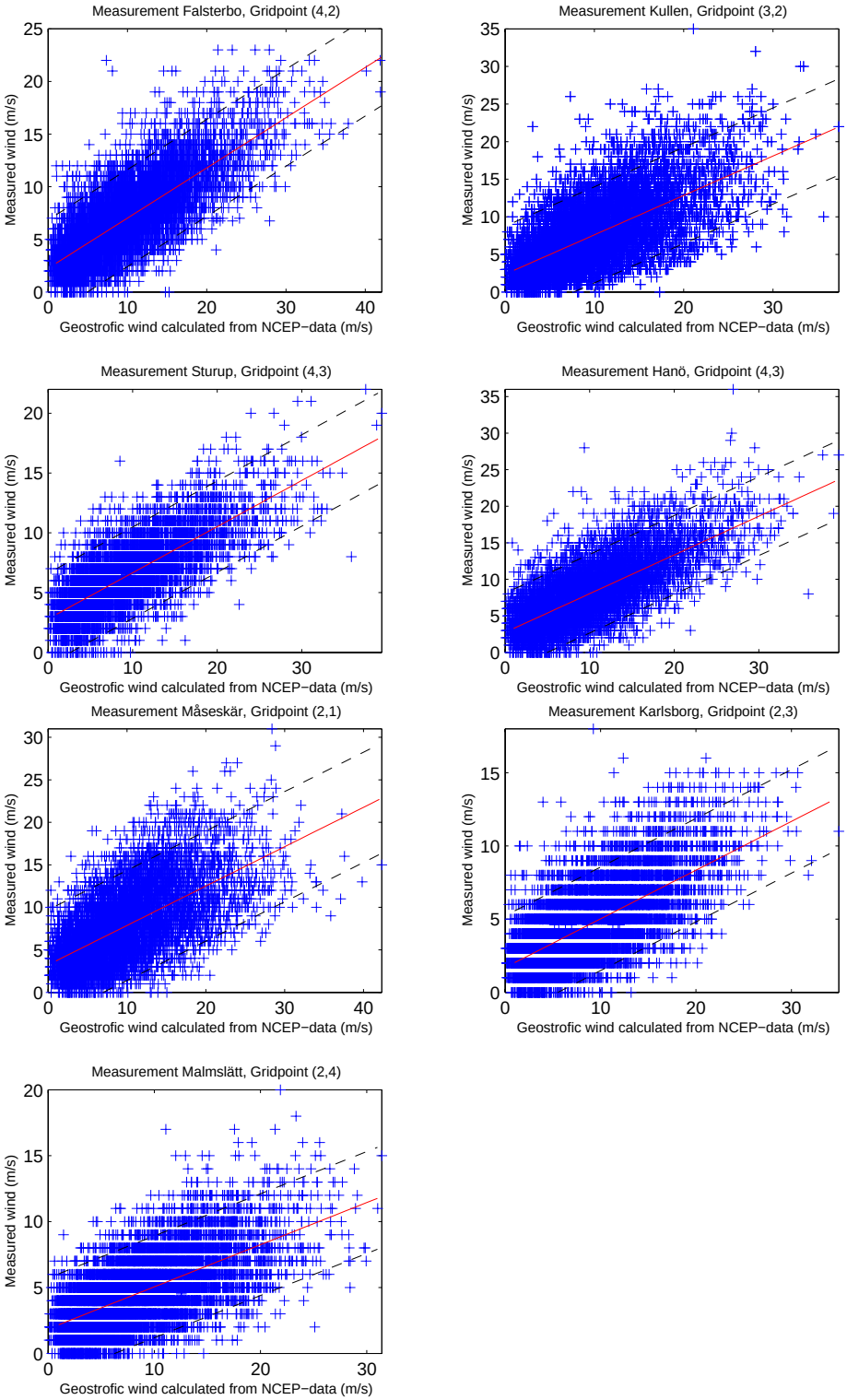

Fig. A3-2: Measurements from ground stations and calculated geostrophic wind at the grid point closest to the ground station at 12z. For geographic locations of grid points and ground stations see map below. Data for ground stations in Falsterbo, Kullen, Hanö Automatic Station, Måseskär, Karlsborg and Malmslätt for the period 1961-01-01 to 1990-12-31 and in Sturup from 1972-12-01 to 1990-12-31 from SMHI, Norrköping.

Tab. A3-2: The coefficients for the regression line (y=ax+b) with 95% confidence interval, standard deviation (s), correlation between measurements and calculated geostrophic wind (Corr) at ground stations close to wind grid points.

Ground Station	Gridpt	a±e	b±e	s	Corr
Falsterbo	4 2	0.4771 ± 0.0039	2.246 ± 0.023	2.35	0.76
Kullen	3 2	0.5240 ± 0.0056	2.363 ± 0.031	3.26	0.66
Sturup	4 3	0.3857 ± 0.0041	2.806 ± 0.024	1.95	0.75
Hanö Automat	4 3	0.5298 ± 0.0047	2.742 ± 0.026	2.75	0.73
Måseskär	2 1	0.4632 ± 0.0057	3.238 ± 0.032	3.30	0.62
Karlsborg	2 3	0.3326 ± 0.0034	1.697 ± 0.017	1.80	0.68
Malmslätt	2 4	0.3197 ± 0.0039	1.856 ± 0.019	1.97	0.63

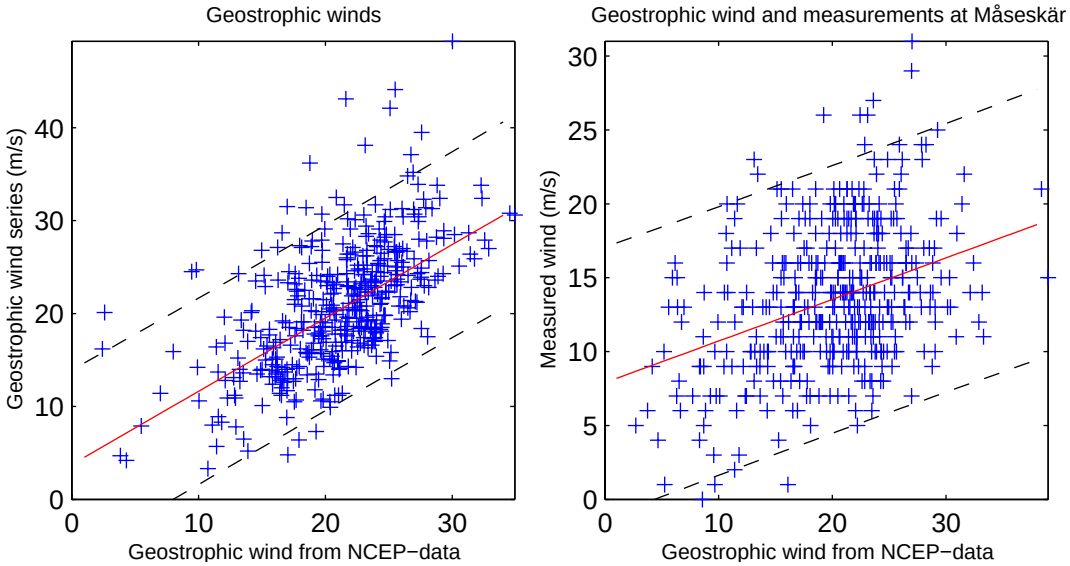

Fig. A3-3: Left: Days with geostrophic wind calculated from NCEP-data exceeding 25 m/s in any grid point. Plot for NCEP-wind value at wind grid point (3,3) (close to Ljungby) and for geostrophic wind calculated from pressure measurements. a=0.79±0.05, b=3.72±0.59, s=5.08 and Corr=0.59.
Right: Days with geostrophic wind calculated from NCEP-data exceeding 25 m/s in any grid point. Plot of NCEP-wind at wind grid point(2,1) and of measured wind at 12z on Måseskär. a=0.28±0.04, b= 7.90±0.22, s=4.62 and Corr=0.37.

Appendix 4. NCEP-Cluster

Mean pressure pattern for each cluster derived from days in NCEP-data with geostrophic wind exceeding 25 m/s in any wind grid point.

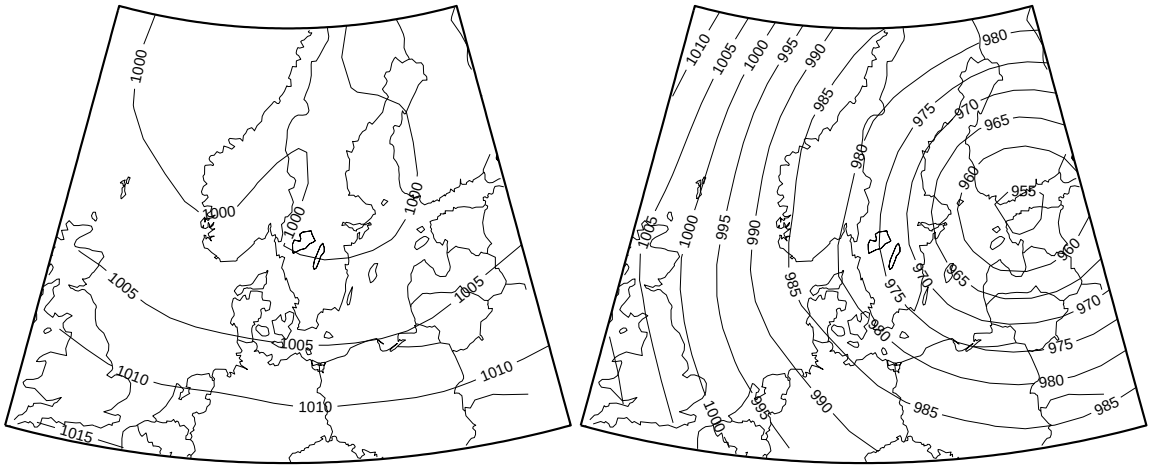

1

2

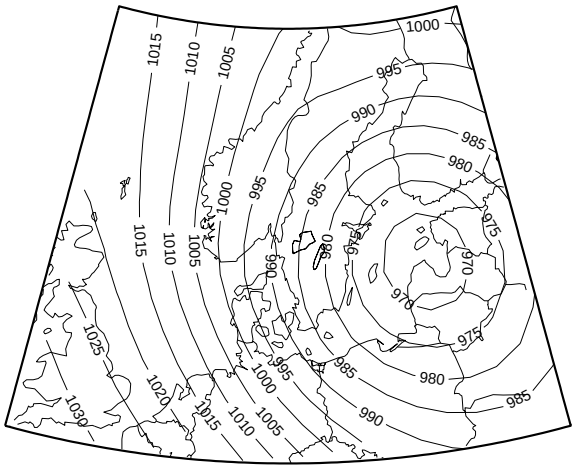

3

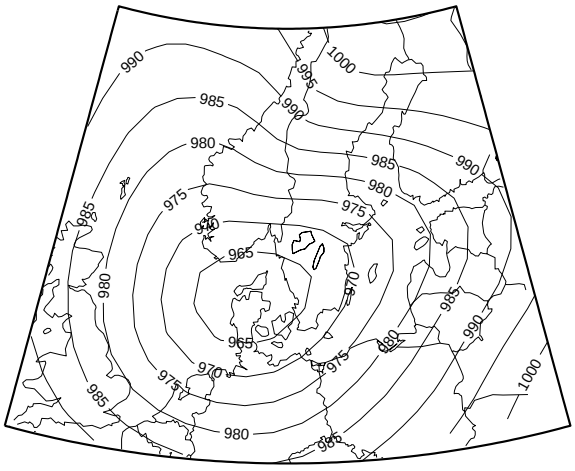

4

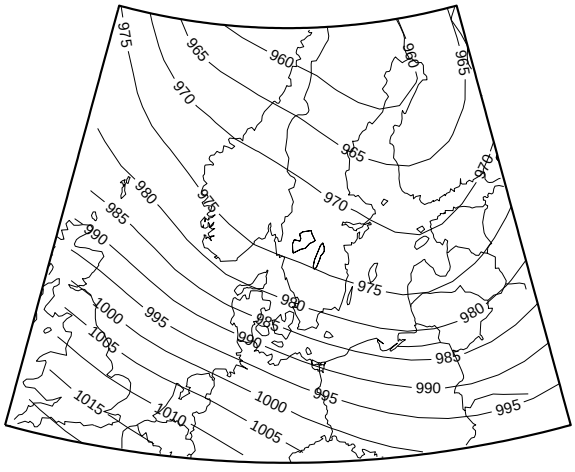

5

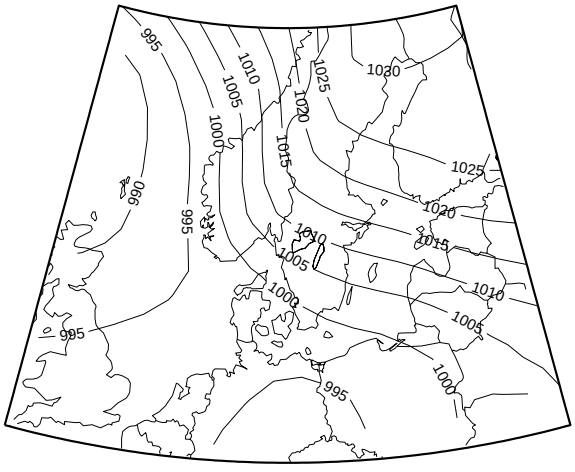

6

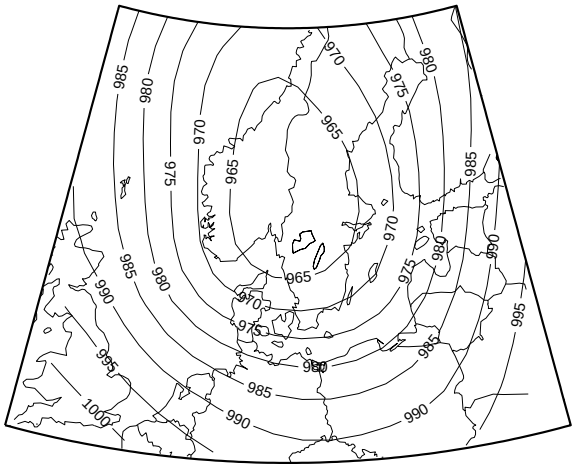

6

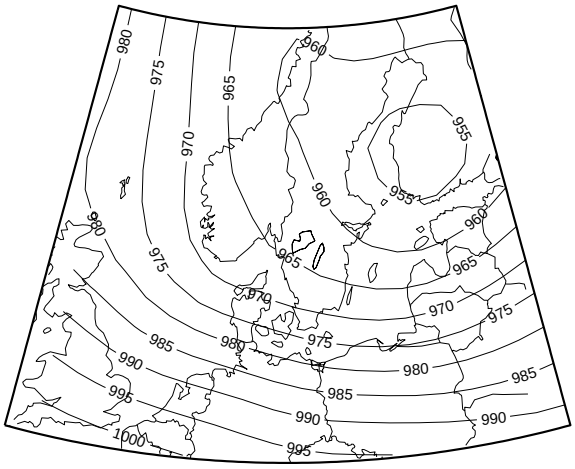

8

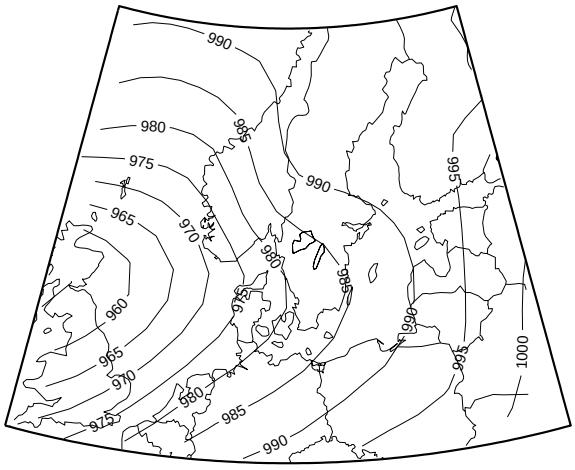

9

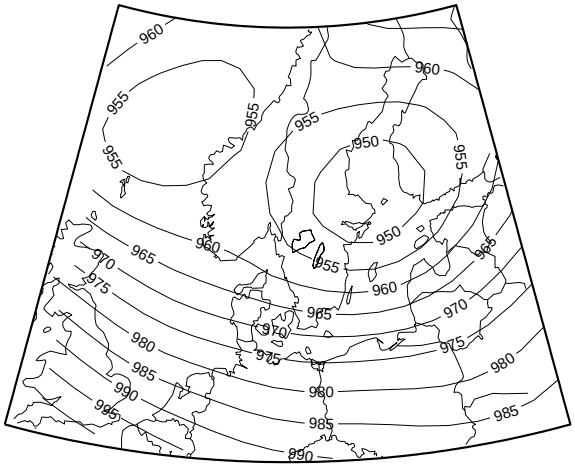

10

Appendix 5. Main Principal Components

In this appendix the ten first principal components are plotted. Each column contains the PC:s derived from storm days in NCEP-data, HadAM3COM-data and HadAM3A2-data. The first 3 PC:s have a contour interval of 0.02, number 3-7 interval 0.05.

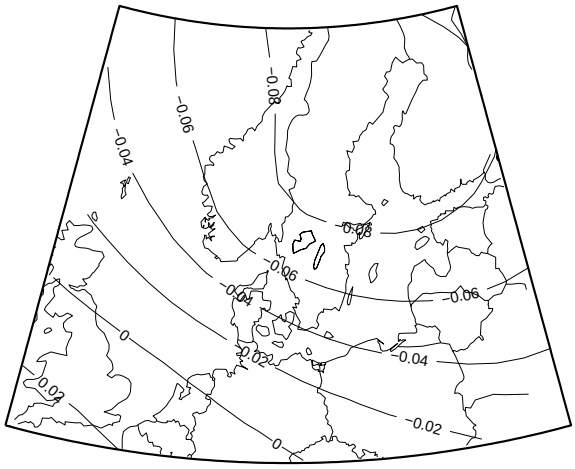

NCEP PC 1

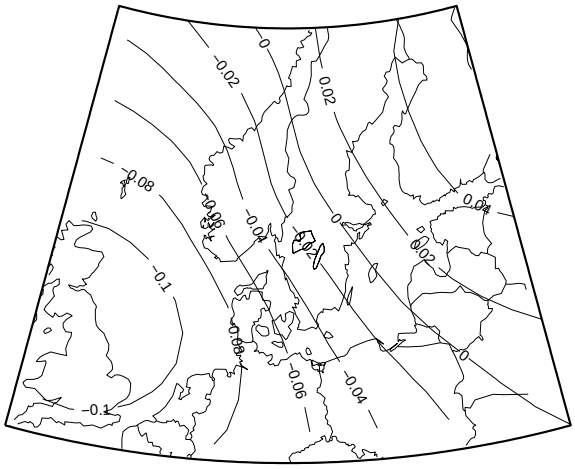

NCEP PC 2

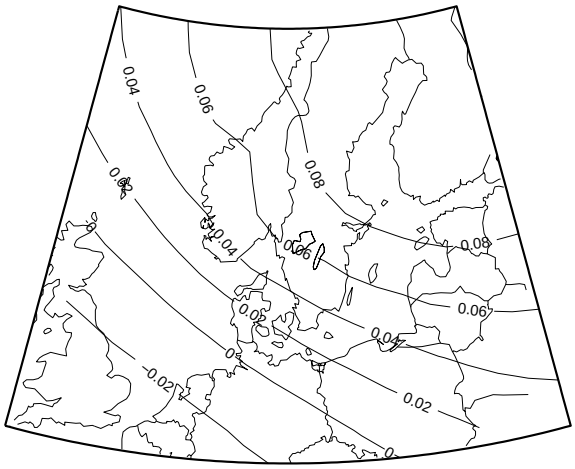

COM PC 1

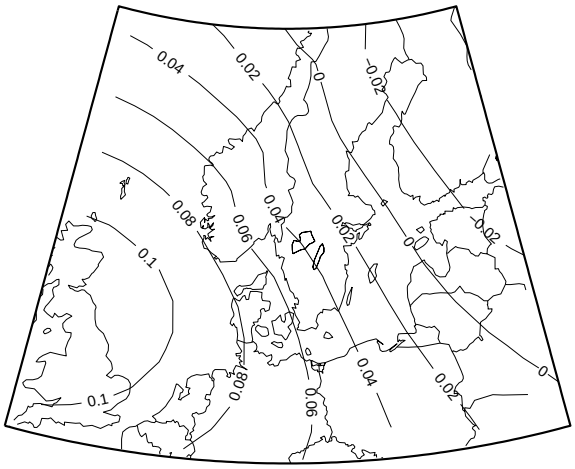

COM PC 2

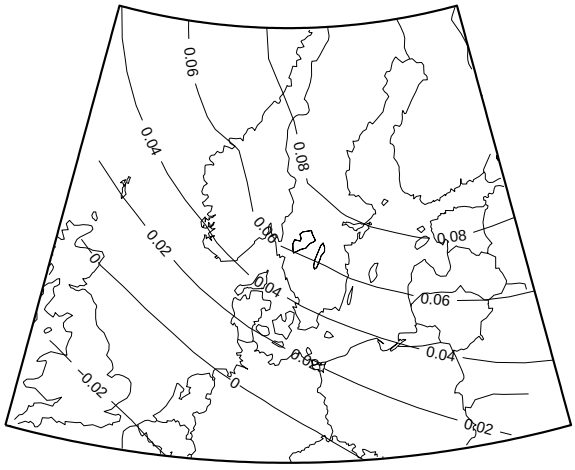

AM2 PC1

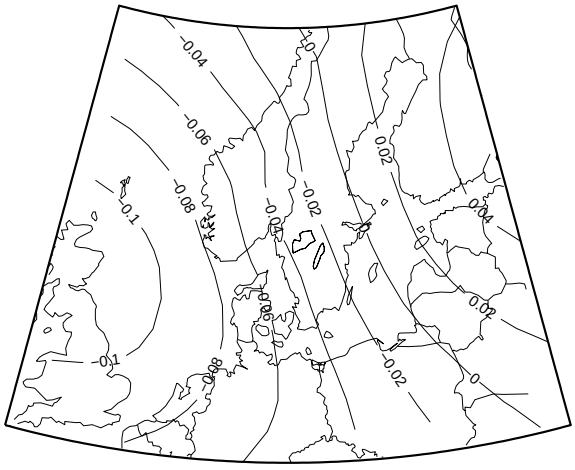

AM2 PC2

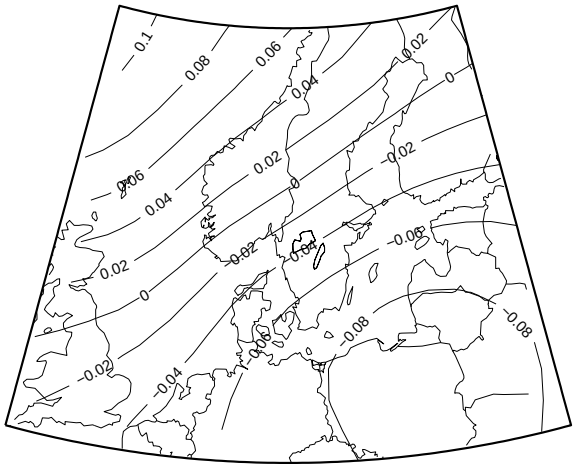

NCEP PC 3

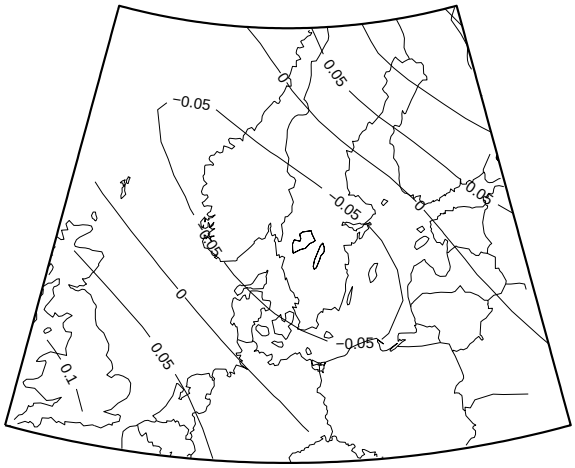

NCEP PC 4

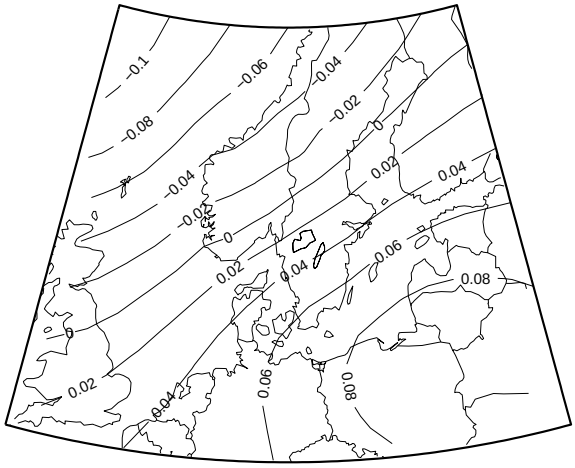

COM PC 3

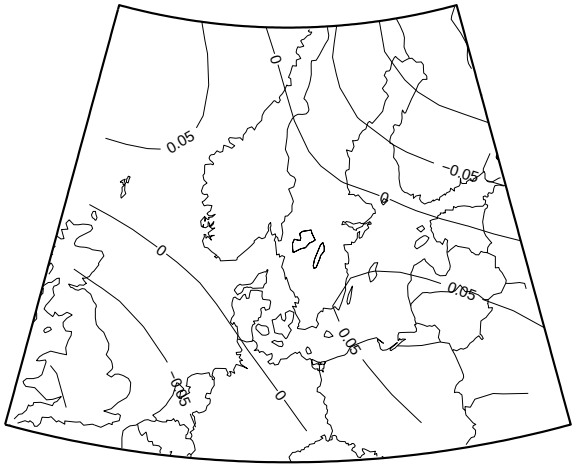

COM PC 4

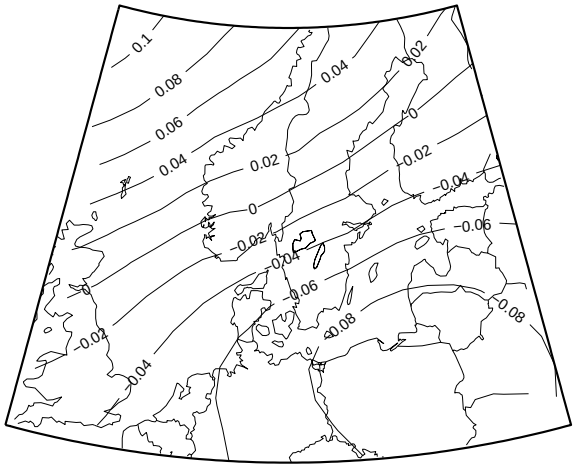

AM2 PC 3

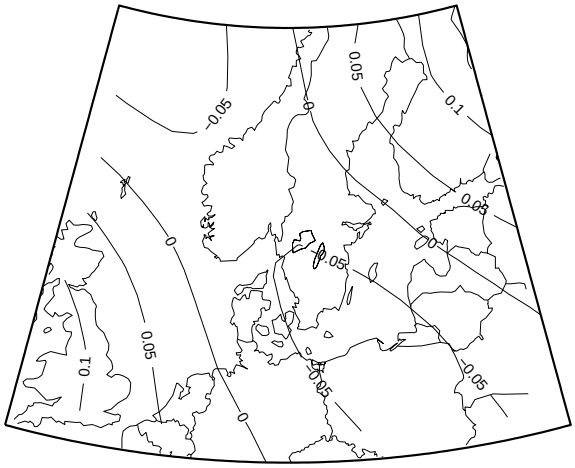

AM2 PC4

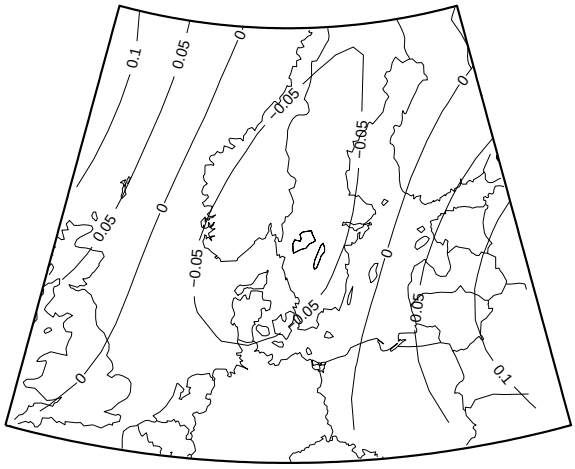

NCEP PC 5

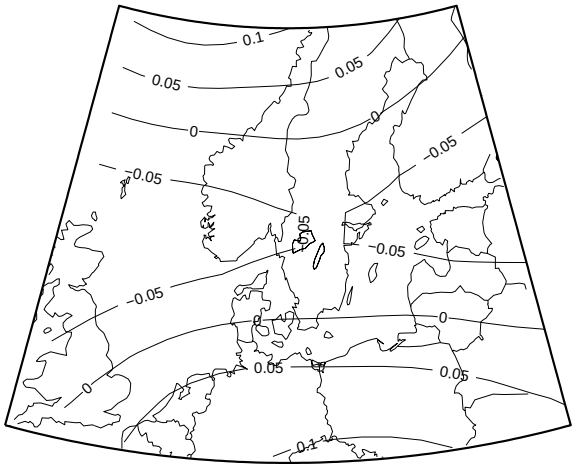

NCEP PC 6

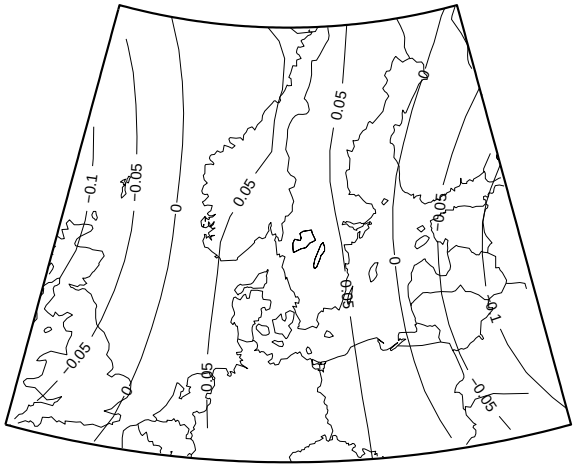

COM PC 5

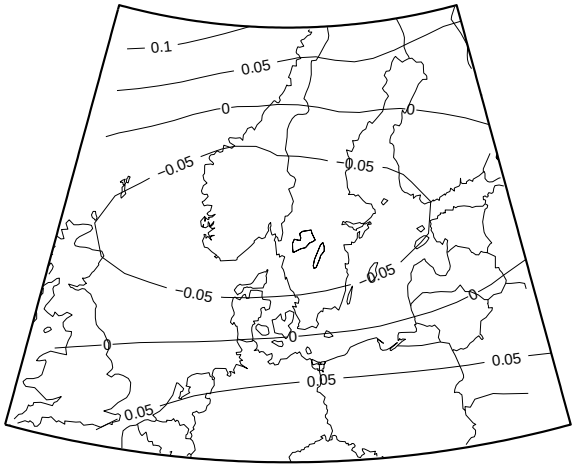

COM PC 6

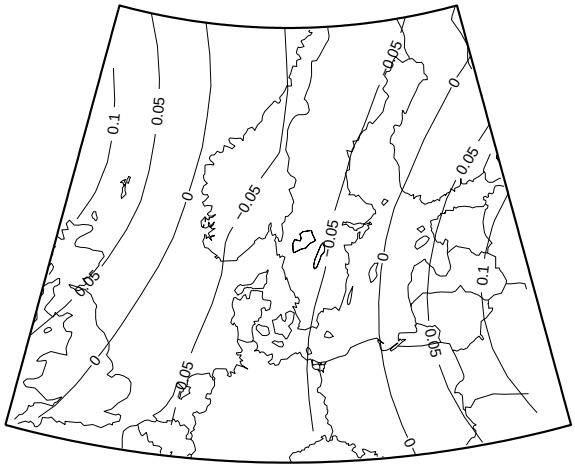

A2 PC 5

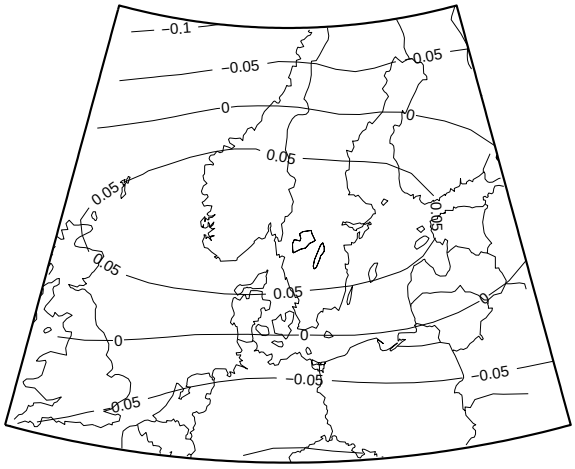

A2 PC 6

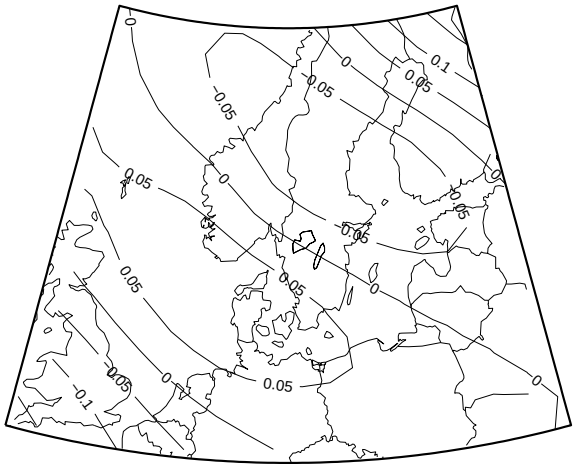

NCEP PC 7

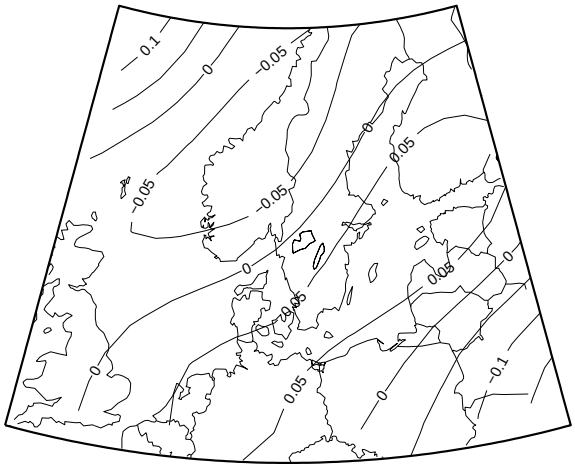

NCEP PC 8

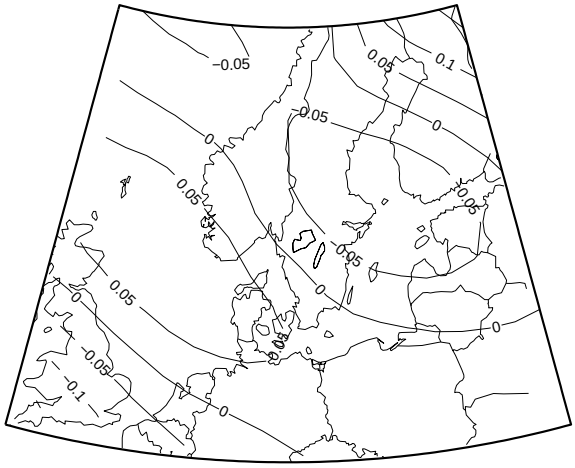

COM PC 7

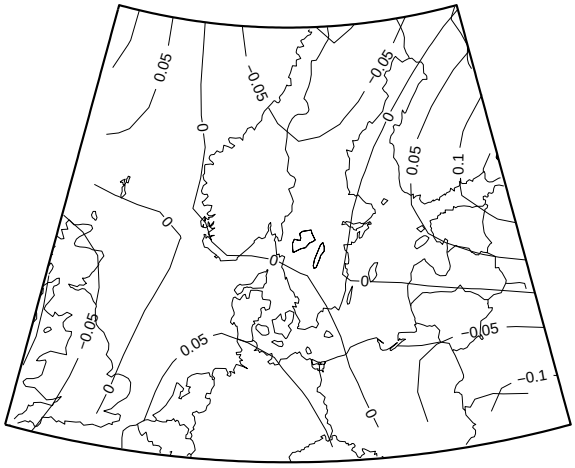

COM PC 8

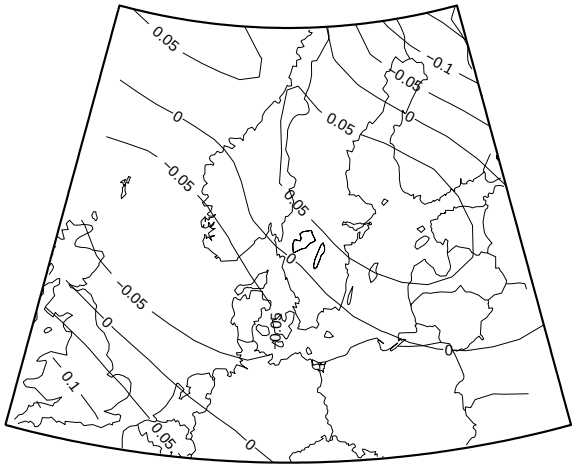

A2 PC 7

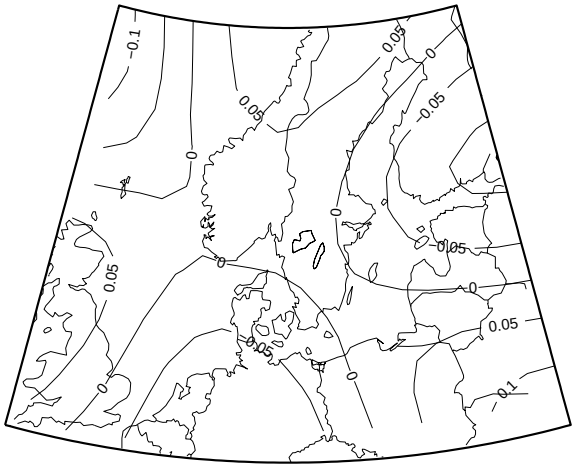

A2 PC 8

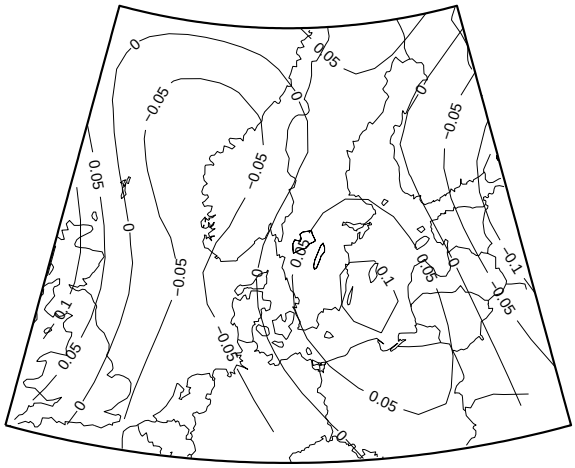

NCEP PC 9

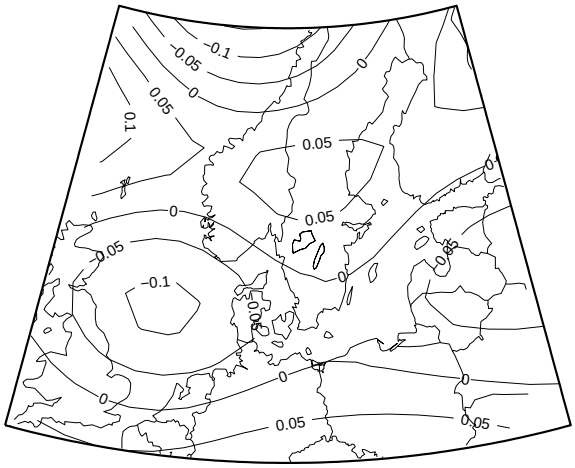

NCEP PC 10

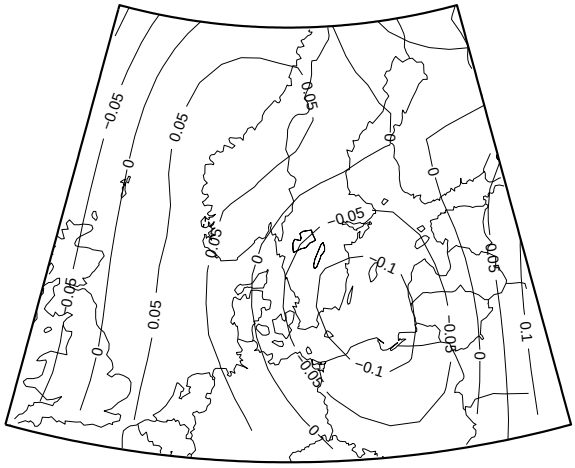

COM PC 9

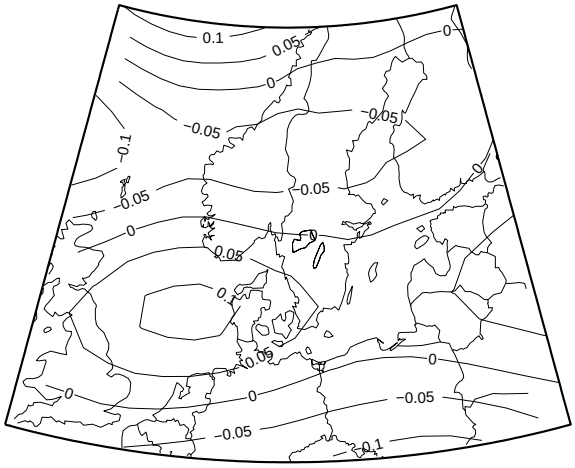

COM PC 10

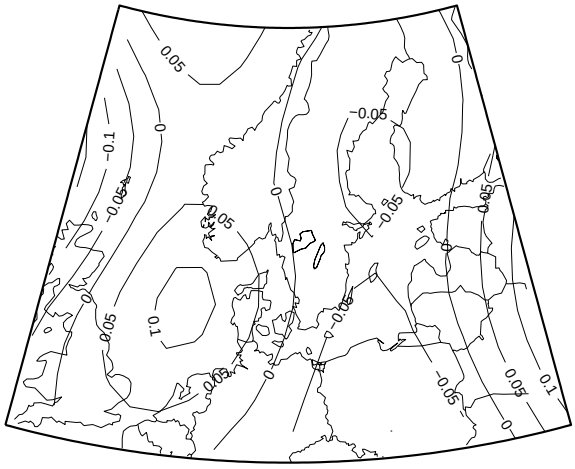

A2 PC 9

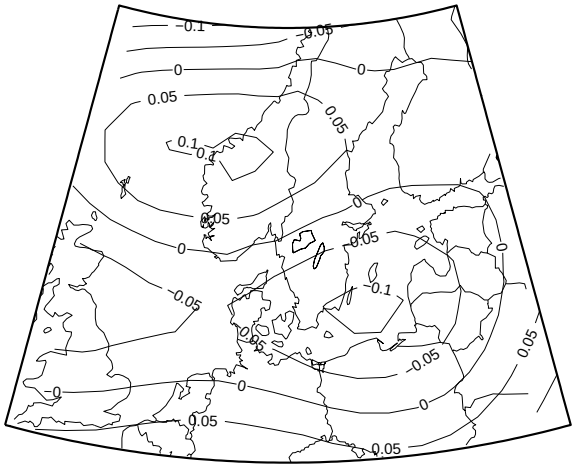

A2 PC 10

Mean pressure value of days associated with winds exceeding 25 m/s

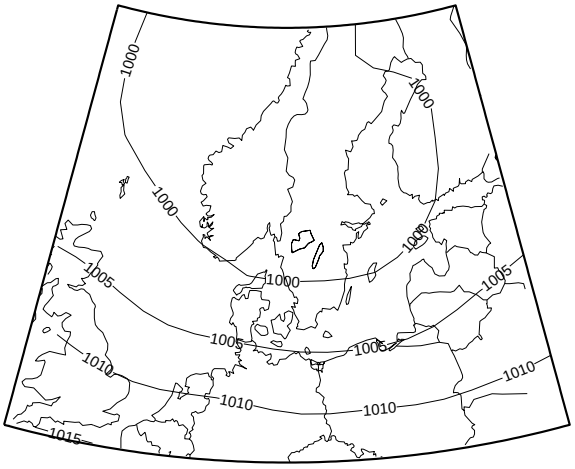

NCEP

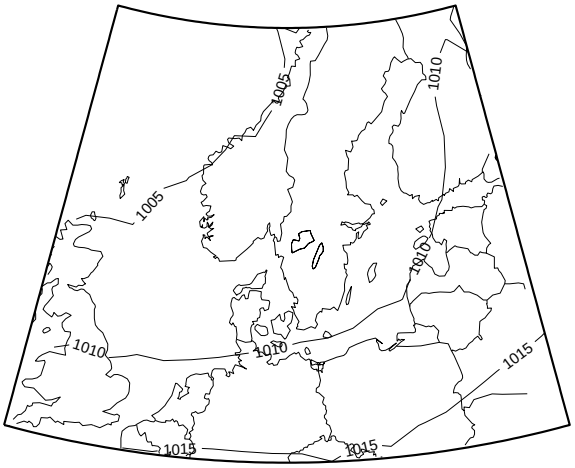

COM

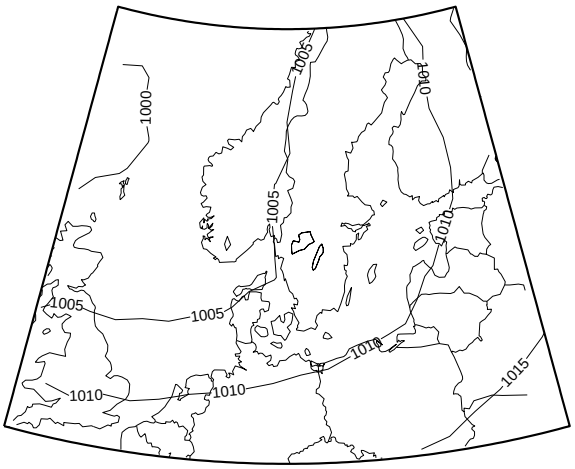

A2

Appendix 6. Cluster based on 29 stormy days

Mean value of pressure for each cluster based on 29 days with observed strong winds.

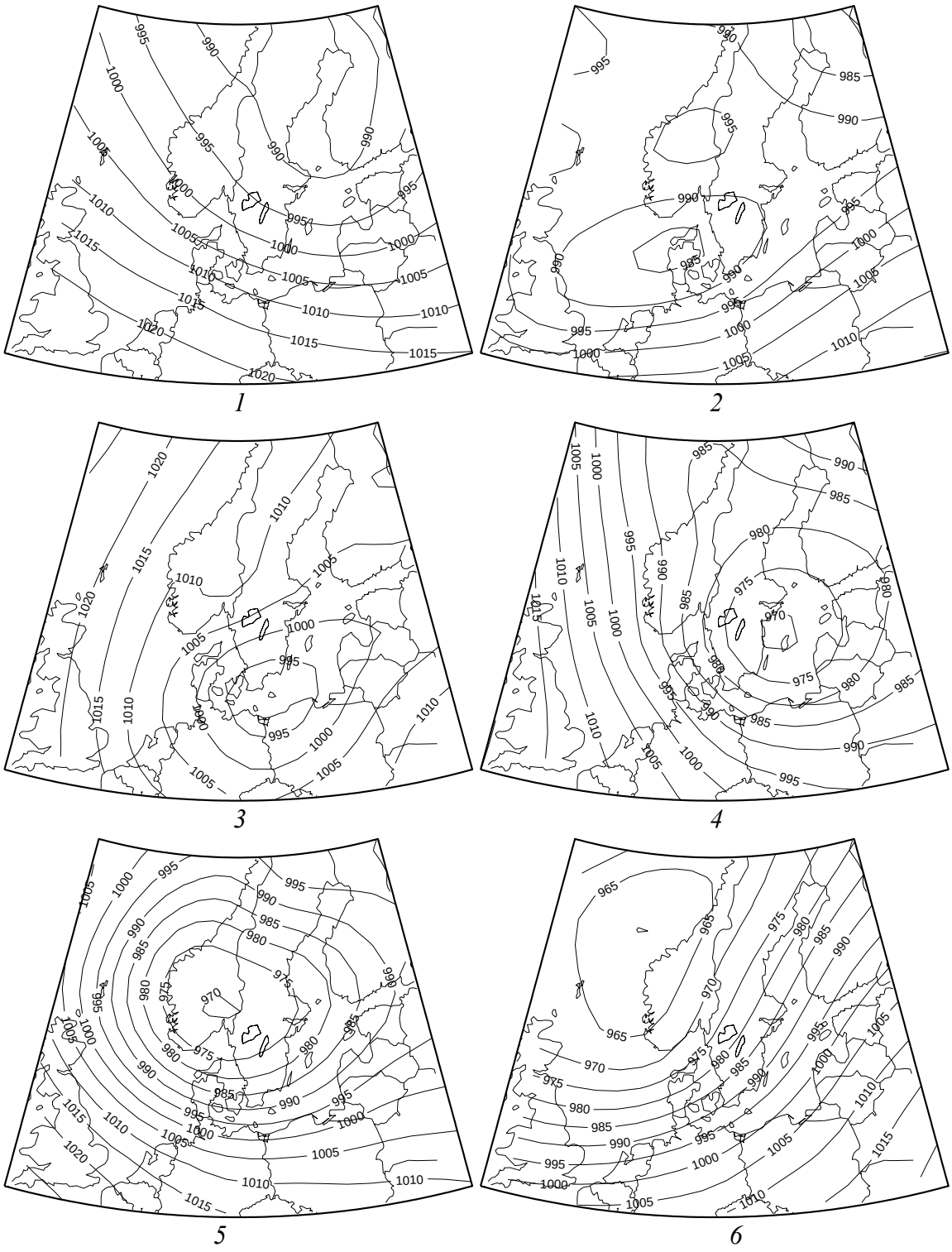

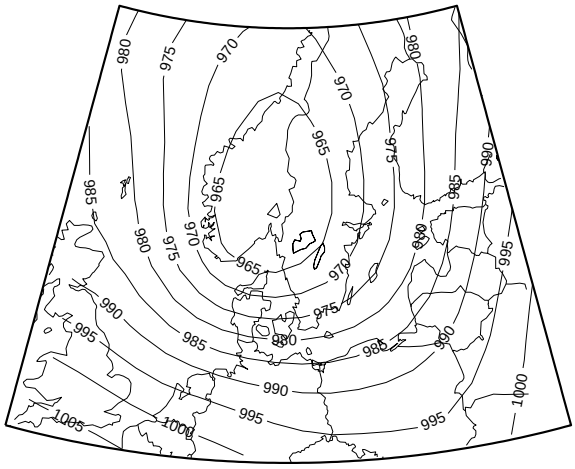
980
975
970
965
970
975
980
985
990
995
1000
1005

7

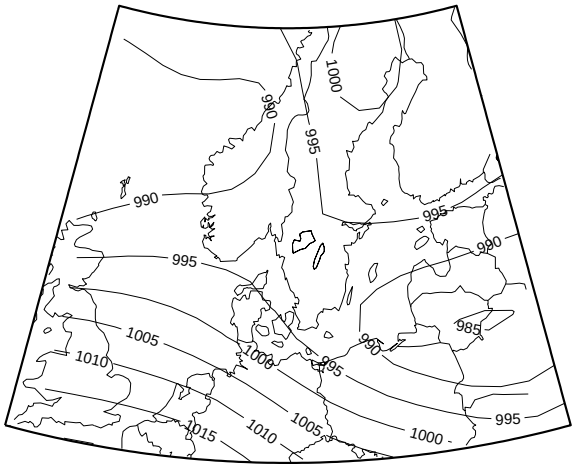
1000
995
990
995
990
995
985
1005
1010
1015
1010
1005
1000
995

8

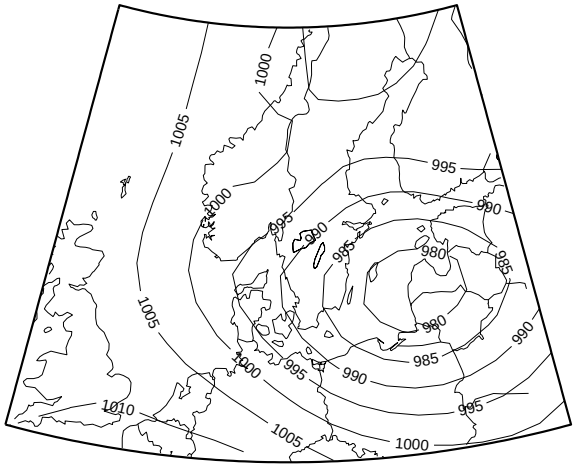
1000
1005
995
990
995
990
980
985
1000
995
990
985
980
990
995
1000
1005
1010

9

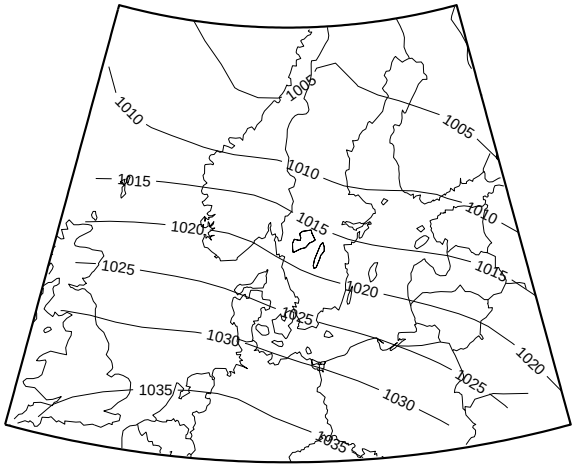
1010
1005
1010
1015
1020
1015
1010
1025
1020
1025
1030
1025
1020
1035
1030
1035

10

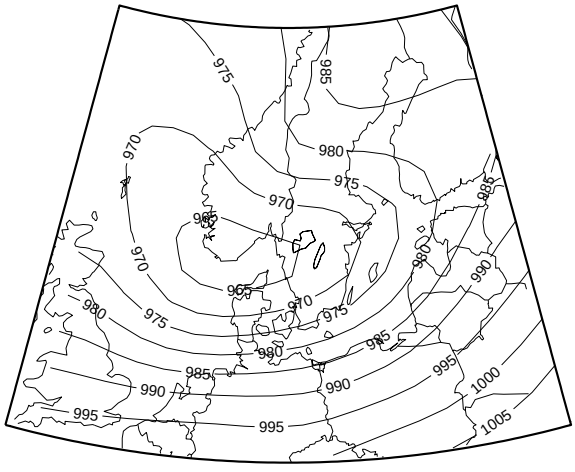
975
985
970
980
975
970
985
980
970
965
970
975
980
985
990
985
990
995
1000
995
1005

11

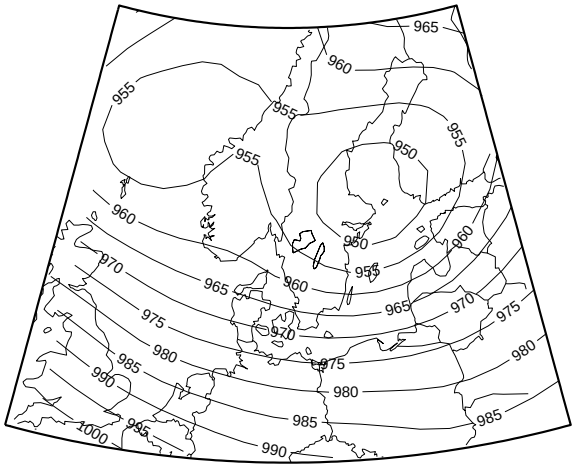
965
960
955
955
950
955
955
960
960
960
970
965
960
965
970
975
975
970
980
985
980
985
990
995

12

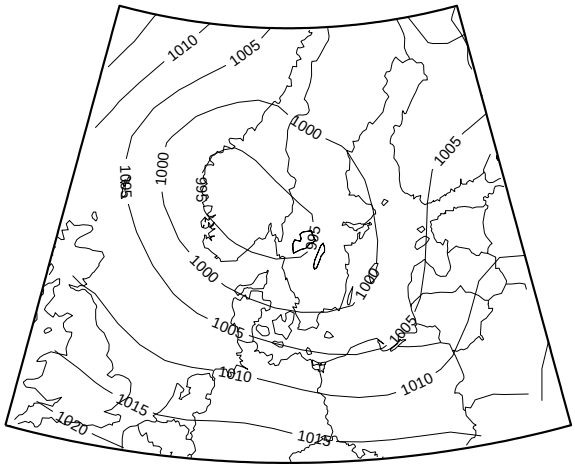
1010
1005
1000
995
1000
1005
1010
1015
1020

13

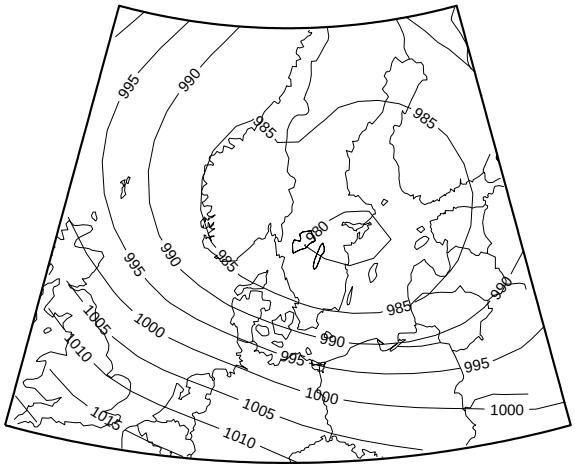
995
990
985
980
985
990
995
1000
1005
1010
1015

14

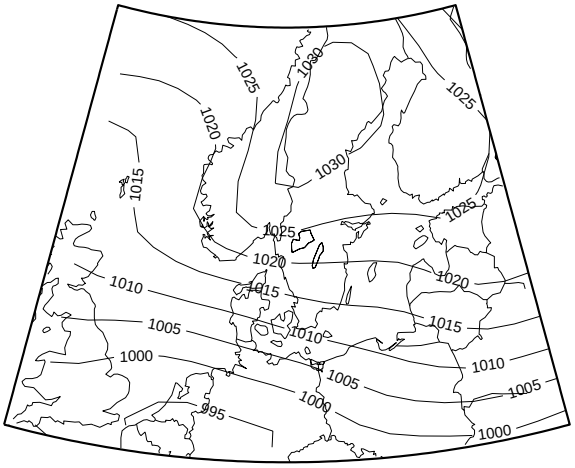
1025
1030
1020
1015
1010
1005
1000
995

15

Appendix 7. Days not classified in HadAM3COM and HadAM3A2

Days associated to geostrophic wind exceeding 25 m/s that did not fulfill a threshold value of 0.70 to the NCEP cluster days in HadAM3COM and HadAM3A2 were clustered. Here are the most frequent clusters. A decrease in clusters associated with a Northerly/Easterly high is seen. The frequency of each cluster is found in the figure text.

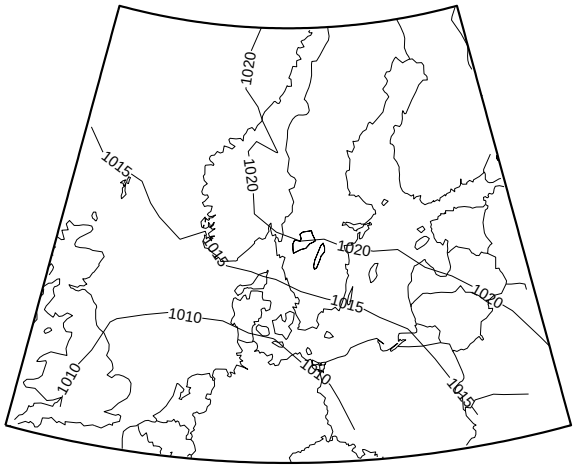

67 of 83 in HadAM3COM

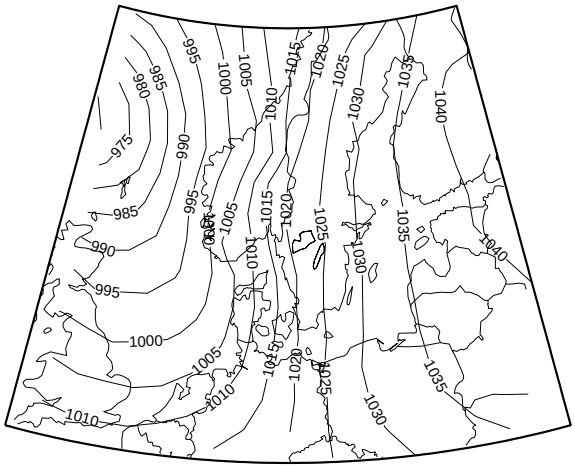

6 of 83 in HadAM3COM

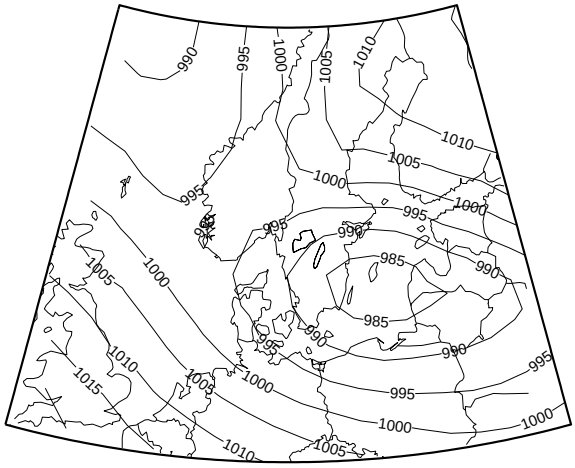

47 of 81 in HadAM3A2

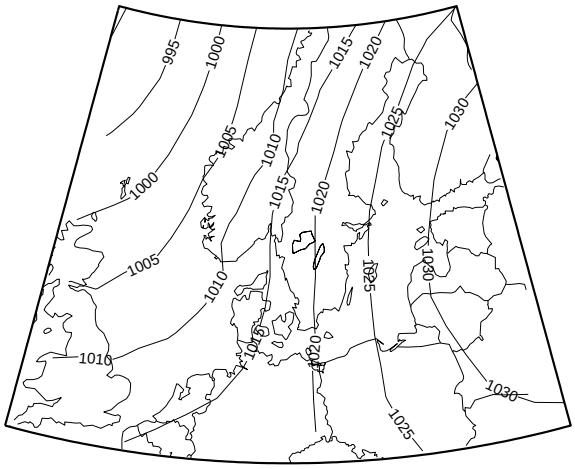

23 of 81 in HadAM3A2